5-31-1987

Studies directed toward beta-cyclodextrin and capped beta-cyclodextrin mimics of alpha-chymotrypsin

Preston Marlon Canzius
New Jersey Institute of Technology

Copyright Warning & Restrictions

The copyright law of the United States (Title 17, United States Code) governs the making of photocopies or other reproductions of copyrighted material.

Under certain conditions specified in the law, libraries and archives are authorized to furnish a photocopy or other reproduction. One of these specified conditions is that the photocopy or reproduction is not to be "used for any purpose other than private study, scholarship, or research." If a, user makes a request for, or later uses, a photocopy or reproduction for purposes in excess of "fair use" that user may be liable for copyright infringement,

This institution reserves the right to refuse to accept a copying order if, in its judgment, fulfillment of the order would involve violation of copyright law.

Please Note: The author retains the copyright while the New Jersey Institute of Technology reserves the right to distribute this thesis or dissertation

Printing note: If you do not wish to print this page, then select "Pages from: first page # to: last page #" on the print dialog screen

ABSTRACT

Title of Thesis: STUDIES DIRECTED TOWARD BETA-CYCLODEXTRIN AND CAPPED BETA-CYCLODEXTRIN MIMICS OF ALPHA-CHYMOTRYPSIN

Preston M. Canzius, Master of Science, 1987

Thesis directed by: Dr. Carol A. Venanzi

Molecular mechanics calculations were used to investigate beta-cyclodextrin and capped beta-cyclodextrin as models for the active site of alpha-chymotrypsin. The Amber molecular mechanics force field was used to investigate the effect that addition of the caps has on the conformation of the beta-cyclodextrin macrocycle.

The RMS module of Amber was used to calculate differences in position between the atoms of the minimized mimics and those of the X-ray crystal structure. The deviation in position of the atoms of the minimized capped beta-cyclodextrin macrocycle was found to be larger than that of the minimized beta-cyclodextrin, indicating that the caps do affect the conformation of the macrocycle. Molecular electrostatic potential maps calculated in planes parallel to the average plane of the glycosidic oxygen atoms indicated that the addition of the caps to the beta-cyclodextrin macrocycle alters the pattern of the map in each plane. However, the general qualitative features of the beta-cyclodextrin and capped beta-cyclodextrin maps are similar.

STUDIES DIRECTED TOWARD BETA-CYCLODEXTRIN

AND

CAPPED BETA-CYCLODEXTRIN MIMICS OF ALPHA-CHYMOTRYPSIN

by

PRESTON M. CANZIUS

Thesis submitted to the Faculty of the Graduate School of the New Jersey Institute of Technology in partial fulfillment of the requirement for the degree of Master of Science in Chemical Engineering

1987

APPROVAL

Title of Thesis: STUDIES DIRECTED TOWARD BETA-CYCLODEXTRIN AND CAPPED BETA-CYCLODEXTRIN MIMICS OF ALPHA-CHYMOTRYPSIN

Name of Candidate: PRESTON M. CANZIUS

Thesis and Abstract Approved: _____ _____

Dr. CAROL A. VENANZI Date

Department of Chemistry

Signatures of other members of the thesis committee:

_____ 5/4/87

Date

_____ 5/4/87

Date

VITA

Name: **Preston Marlon Canzius.**

Permanent address:

Degree and date to be conferred: Master of Engineering Science, 1987

Date of birth:

Place of birth:

Secondary education: Seton Hall Preparatory School, 1979

Collegiate institutions attended	Dates	Degree	Date of Degree
New Jersey Institute of Technology	1980-1985	B.S.	1985
New Jersey Institute of Technology	1985-1987	M.S.	1987

Major: Chemical Engineering

Publication: Canzius, P.M. Bull. Am. Phys. Soc. 1987, 32, 410.

Positions held: Lab Instructor
Research Assistant
Department of Chemistry and Chemical Eng.
New Jersey Institute of Technology
Newark, N.J. 07102.

TABLE OF CONTENTS

ACKNOWLEDGEMENT

I would like to express my appreciation and gratitude to **Dr. Carol A. Venanzi**, whose assistance and guidance has been instrumental to the success of this study. Thanks are also due to Dr. A. Greenberg and Dr. G. Lewandowski for careful reading of the thesis, and to Wen-Chung Shang for help in preparing some of the figures.

LIST OF TABLES

LIST OF FIGURES

I. INTRODUCTION

A. General Properties of Enzymes and Mimics

Enzymes are proteins capable of catalytic activity. The catalysis occurs in a definite region of the enzyme referred to as the active site or catalytic cleft. The active site is composed of amino acid residues which are known to participate in the catalytic process. The outstanding characteristic of enzyme catalysis is that the enzyme specifically binds its substrate [1], and the reaction occurs at speeds on the order of a billion times the speed of the uncatalyzed reaction [2].

In an attempt to elucidate the mechanism of enzyme-substrate interactions, several research groups [3,4,5] have begun the design and synthesis of artificial enzymes. These artificial enzymes mimic the substrate selectivity and high reaction velocity inherent in most enzyme-substrate interactions during catalysis. Substituents containing functional groups similar to the catalytic residues of enzymes have been added to the macrocyclic templates of, for example, cyclic urea, cyclodextrin, or crown ether artificial enzymes. The macrocycles provide the complexation site, while the molecular architecture of the mimic is designed to hold the catalytic functional groups in position for optimal interaction with the substrate.

Recent work by Bender [3], Breslow [4], and Cram [5] has focused on the design of compounds that contain reactive hydroxyl groups that mimic the action of Serine-195 of

chymotrypsin in acyl transfer to the substrate. These research groups have been able to achieve enzymatic reaction velocities with their cyclodextrin [3], capped cyclodextrin [4], and cyclic urea mimics [5], respectively.

B. Mechanism of Alpha-Chymotrypsin Catalysis

Alpha-chymotrypsin belongs to the serine protease family of enzymes. It is one of the most studied enzymes and much is known about its catalytic mechanism from crystallographic and dynamical studies. Its physiological function is to catalyze the hydrolysis of peptide bonds of protein food in the intestines of mammals. The enzyme has a specificity for aromatic amino acids in that it cleaves proteins on the carboxyl side of the aromatic amino acids. The active site consists of the catalytic triad Ser-195, Asp-102, and His-57, as well as several hydrophobic residues. The catalytic activity of chymotrypsin depends on the unusual reactivity of Ser-195. Generally, a $-CH_2OH$ group is quite unreactive under physiological conditions [1]. An explanation has emerged from X-ray studies of the three-dimensional structure of the enzyme [6]. The X-ray structure indicates that His-57 is adjacent to Ser-195. In addition, the carboxyl side chain of Asp-102 is in proximity to His-57 (Figure 1). Asp-102 is hydrogen bonded to His-57 which is also hydrogen bonded to Ser-195, forming the charge relay network (Figure 2) [6]. Generally, a hydrophilic residue like Asp-102 would be found on the surface of the

enzyme, rather than buried within the active site. Its unique juxtaposition with the unusually polarizable system of the imidazole ring (His-57) seems to be the key to the activity of this enzyme. The function of the negatively-charged Asp-102 group is to polarize the imidazole ring. This gives a possibility of proton transfer along hydrogen bonds, to allow the hydroxyl proton of Ser-195 to be transferred to His-57. The active serine residue becomes then a reactive nucleophile capable of attacking the scissile peptide bond [1].

The catalytic efficiency of alpha-chymotrypsin cannot be solely attributed to the presence of the charge relay network. X-ray, NMR (nuclear magnetic resonance), and other studies have indicated that many factors operate during the catalytic process. Several specific enzyme-substrate interactions have been identified in making the process more efficient. For example, stabilization of the tetrahedral intermediate, and thus lowering of the transition state barrier, is accomplished by hydrogen bond formation of the substrate carbonyl functionality with the amide hydrogen of Ser-195 and Gly-193 [1]. Peptide bond hydrolysis begins with an attack by the oxygen atom of the hydroxyl group of Ser-195 on the carbonyl carbon atom of the susceptible peptide bond [6]. The carbon-oxygen bond of this carbonyl group becomes a single bond and the oxygen atom acquires a net charge [1]. The four atoms bonded to the carbonyl carbon form a transient tetrahedral intermediate which is facilitated by hydrogen bonds between the negatively charged

carboxyl oxygen atom and two main chain NH groups (Figure 3) [6]. The transfer of a proton from Ser-195 to His-57 is also essential for the formation of the tetrahedral transition state (Figure 4). Asp-102 then orients the imidazole ring of His-57 and partially neutralizes the charge on this ring that develops during the transition state. The proton stored by the His-Asp couple is then donated to the nitrogen atom of the substrate. This results in cleavage of the bond. At this point, the amine component is hydrogen bonded to His-57, while the acid portion is esterified to Ser-195 [7]. This step essentially marks the culmination of the acylation step of the hydrolysis mechanism.

The next step of the hydrolysis mechanism is deacylation (Figure 5). The amine component of the substrate diffuses away, and a water molecule takes it place at the active site. The charge relay network acquires a proton from water. The resulting hydroxide ion then attacks the carbonyl carbon of the acyl group attached to Ser-195. His-57 donates a proton to the oxygen atom of Ser-195, which results in the release of the acid component (product) of the substrate [7]. The acid component diffuses away and the enzyme is ready for another round of catalysis. This concludes the deacylation portion of the hydrolysis mechanism.

C. Computer Modeling of Biomimetic Catalysts

The use of computer modeling of biomimetic catalysts to further the understanding of enzyme-substrate interactions is facilitated by high speed computers, a myriad of software packages, and the availability of high resolution graphics terminals. Enzyme mimics have been modeled by Venanzi and coworkers using such techniques as molecular mechanics to estimate the conformational properties of the uncomplexed and complexed cyclic urea mimics of chymotrypsin [8,9]. Molecular mechanics calculations were used to calculate the conformational properties of a cyclic urea mimic proposed, but not yet synthesized, by Cram and coworkers [5b]. The Amber molecular mechanics force field was used to calculate the uncomplexed and complexed structures of a cation-binding mimic precursor compound [8], as well as the structure of the cyclic urea compound containing substituents which mimic the action of the catalytic triad in chymotrypsin [9,10]. Venanzi and coworkers found that, in order to bring the structural elements of the catalytic triad into a spatial orientation suitable for the proton transfer, the proposed mimic would have to adopt a highly strained conformation. Computer graphics modeling was used to optimize positioning of the catalytic substituents around the mimic. This method was used to redesign the strained portion of the molecular architecture. Several alternative mimics that had the catalytic triad in a "favourable" position were suggested. The "best" structure of the two alternatives, as found by Venanzi and Bunce [9], was the

mimic that contained a fused ring which positioned the components at a reasonable distance for proton transfer.

It is known that electrostatic forces play a major part in the initial phase of an enzyme-substrate interaction [11]. Computer modeling can also provide the molecular recognition pattern of the enzyme (mimic) for the substrate through the use of molecular electrostatic potential contour maps [8,9,10]. Venanzi and Bunce [8] have shown that the electrostatic potential contour maps can qualitatively indicate the electrostatic complementarity of the enzyme mimic for the substrate. In addition, the electrostatic potential pattern was shown to determine the directionality of approach of the substrate into the binding cavity [8, 9, 10].

D. Cyclodextrins as Biomimetic Catalysts

Cyclodextrins are torus-shaped oligosaccharides formed by glucose units that are covalently bonded by glycosidic 1->4 linkages. They can be obtained by enzymatic degradation of starch. The important structural features in these compounds are their toroidal shape, hydrophobic cavity, outer surface, and hydrophilic faces [12]. The numbering scheme of the glucose fragment used in the present study is shown in Figure 6, while the orientation of the primary and secondary hydroxyl groups is shown in Figure 7. The primary hydroxyl groups at the O11 position of a glucose unit form the narrow face (between 6.5 A and 7 A),

at the "bottom" of the macrocycle, while the secondary hydroxyl groups at the O3 and O6 positions form a somewhat wider face (appromimately 7 A), at the "top" [3] (Figure 7). The interior of the cavity contains a ring of C-H groups, a ring of glycosidic oxygens, and another ring of C-H groups (Figure 8). Thus, the interior of the macrocycle has hydrophobic properties; a situation which is analagous to the binding sites of most enzymes.

One of the principal reasons for the utilization of cyclodextrin as an enzyme mimic is the formation of inclusion complexes between the catalyst and substrate, preceeding catalysis. This phenomenon is comparable to the formation of a Michaelis-Menten complex in enzymatic reactions. In addition to complex formation, the resemblance between cyclodextrin-catalyzed and enzymatic reactions includes the following: (1) Both reactions are carried out usually in an aqueous medium; (2) Both reactions show specificity to both substrate and product; and (3) Both reactions show D, L specificity [3].

Cyclodextrins have been used to catalyze the hydrolysis of phenylacetates, organic pyrophosphates or penicillin derivatives, and to accelerate diazo couplings [13]. In industrial applications, they are important as stabilizers for light- or oxygen-sensitive substances. They can also improve the storage of toxic substances, or the solubility of hydrophobic molecules [14]. Catalysis by cyclodextrins may be divided into two categories: (1) Catalysis by the hydroxyl groups, in which the hydroxyl

groups of the cyclodextrin function as an intracomplex catalyst toward the substrate included in the cavity of the macrocycle; and (2) Catalysis by the effect of the reaction field, in which the cavity of the cyclodextrin serves as an apolar and sterically restricted reaction field.

Three kinds of catalysis by the hydroxyl groups of cyclodextrin are known: (a) nucleophilic catalysis; (b) general base catalysis; and (c) general acid catalysis. In nucleophilic catalysis, an anion of a secondary hydroxyl group of the cyclodextrin attacks at the electrophilic center of the ester substrate included in the cavity of the cyclodextrin. This results in the formation of acyl-cyclodextrin (Figure 9), together with the release of the leaving group (Figure 10). The catalysis is completed by the regeneration of the cyclodextrin through a hydrolysis mechanism.

General base catalysis involves enhancement of the nucleophilicity of water molecules by the abstraction of a proton. In the cyclodextrin case, general base catalysis was found for the first time in the hydrolysis of 2,2,2-trifluoroethyl ester of p-nitrobenzoate [14], since no expected covalent intermediate was formed in the course of the reaction and since there is a 1.7 D_2O effect.

There have been no examples of reactions proceeding via general acid catalysis alone by cyclodextrin. In the hydrolysis of trifluoroacetanilide, general acid catalysis

enhances the cleavage of the tetrahedral intermediate formed during nucleophilic attack by a secondary alkoxide ion. General acid catalysis serves to convert the leaving group from an extremely unstable anion of aniline to a stable neutral aniline molecule (Figure 11) [3,15].

Although cyclodextrins are effective as catalysts, their reaction rates generally do not approach those of enzymatic catalysts. Bender [16] has studied the acetylation of a cyclodextrin hydroxyl by bound phenyl acetate esters. Such a reaction can be considered to be a model for the first step in the hydrolysis mechanism of alpha chymotrypsin in which a catalytic serine residue attacks the acyl group of a bound substrate [16]. For the cyclodextrin case, Bender observed Michaelis-Menten kinetics and a maximum velocity for acetyl transfer in the complex which was found to be dependent on hydroxide ion concentration to the first order (Figure 12). Since the substrate can also be cleaved by direct nucleophilic attack by a free hydroxide, the two processes can be compared to give a rate ratio defined by the following equations:

rate of acetyl transfer in the cyclodextrin complex

$$= k_{complex} * [complex] * [OH^-] \quad (1)$$

rate of deacetylation without cyclodextrin

$$= k_{un} * [substrate] * [OH^-] \quad (2)$$

Therefore, the ratio of $k_{complex}/k_{un}$ can be used as a measure of the effectiveness of complexation in promoting deacylation. Enzymes usually approach rate ratios of 10^5 - 10^{10} for the catalyzed versus the uncatalyzed reaction. However, the best rate ratio estimated by Bender [16] for acetyl transfer to beta-cyclodextrin was only 250 using tert-butylphenyl acetate.

Breslow [4], through the use of CPK model-building, has suggested that the substrate of Figure 12 can bind fully in the cavity during the complexation process. However, due to the formation of the tetrahedral transition state the substrate is partially pulled out of the cavity. This could increase the free energy of formation which could cause the complex to decouple and return to cyclodextrin and substrate. Breslow [4] overcame this barrier by modifying not only the beta-cyclodextrin cavity, but also by optimizing the design of the substrate. These two factors enhanced the binding when preceeding from bound substrate through bound transition state and to bound tetrahedral intermediate. Beta-cyclodextrin was modified by replacing the C10 methanol group of each glucose fragment (see Figure 6) with an N,N dimethyl formamide cap (Figure 13). This resulted in a hepta-N-methyl formamide capped beta-cyclodextrin (capped B-CD). Capping of one side of the torus with apolar substituents was shown by Breslow [4] to enhance the binding and catalytic ability of B-CD by a factor of 10^3, due to an increase in the apolar nature of the cavity [4]. Molecular models [4] indicate that the alkyl groups in

the capped B-CD cluster close to the bottom of the cavity, forming an apolar floor on the cavity. The formation of the floor changes the depth of the cavity from 7 A in B-CD to 3.7 A for capped B-CD. It is believed [4] that the larger catalytic rate constant observed with capped B-CD is due primarily to better orientation of the substrate for the nucleophilic attack of the secondary alkoxide ion on the carbonyl carbon atom of the substrate. This change is coupled with a decrease in the binding constants for the binding of phenyl esters. The weaker binding constants can be attributed to too shallow a cavity for the substrate to be fully included during the formation of the inclusion complex [3].

E. Goals of The Present Research

It is the primary goal of the present work to investigate the effect of "capping" on the conformation of the B-CD macrocycle. The conformational and electrostatic molecular recognition properties of B-CD and capped B-CD were studied using the computational procedure described in the Methods Section. This study was undertaken in order to determine: (1) The sensitivity of the calculated energies to scaling of the 1-4 non-bonded terms in the AMBER force field; (2) The relative flexibility of the 1->4 glycosidic linkages of the macrocycle; (3) The degree of structural reorganization that the B-CD macrocycle must undergo in order to accommodate the caps; (4) The effect that the addition of the caps has on the orientation of the secondary

hydroxyl groups around the rim of the macrocycle; (5) The shape and extent of the intrusive floor formed by the caps; and (6) The molecular recognition pattern of the mimic for the substrate, as determined through the use of molecular electrostatic potential contour maps.

II. METHODS

A. Model Building

Beta-cyclodextrin (B-CD) and capped hepta-N methyl formamide beta-cyclodextrin (capped B-CD) were analyzed as models of the active site of alpha-chymotrypsin. The initial structures of the mimics, used as input to the molecular mechanics software package AMBER (Assisted Model Building and Energy Refinement) [17], were built using interactive computer graphics and the molecular modeling facility of Chemgraf/Chem-X [18]. Modeling was accomplished on an Advanced Electronics Design 767 (AED 767) color raster graphics terminal interfaced to a DEC VAX 11/750-785 cluster.

An X-ray crystal structure of the B-CD macrocycle [19], obtained from the Cambridge Crystallographic Database [20] (see Appendix 1), was used as the starting structure for B-CD in the conformational analysis. The coordinates of the X-ray B-CD macrocycle were read into the Chem-X [18] graphics work area. The coordinate file contained coordinates for a 1,4-diazabicyclo(2.2.2)octane substrate and 13 water molecules, in addition to coordinates for the B-CD macrocycle. The substrate and water molecules were subsequently deleted from the graphics work area by the "MODIFY/CURSOR KILL" command of Chem-X [18]. A glucose fragment was then taken from the X-ray crystal structure of the B-CD macrocycle by using the "MODIFY/CURSOR BREAK" command of Chem-X [18]. The "MODIFY/CURSOR ADD HYDROGENS"

command of Chem-X was used to add hydrogens (at a bond distance of 1.0 A) to the carbon and oxygen atoms of the glucose fragment. The coordinates of this fragment were then written out with the "WRITE FOREIGN" command, in a format compatible with the input format of GAUSSIAN 80 UCSF. The glucose fragment was then used as input to GAUSSIAN 80 UCSF in order to determine "potential derived" atomic point charges (refer to Section C). This fragment supplied a set of atomic point charges and "dummy" input coordinates for the glucose fragment used in the PREP module of AMBER [17].

PREP is designed to provide a convenient means of building residues that can be later linked together to form a molecular system. The input to PREP consists of atom types, atom names, cartesian coordinates, and atomic point charges. PREP converts the cartesian coordinates to internal coordinates. Internal coordinates differ from cartesian coordinates in that cartesian coordinates use x, y, and z-coordinates to describe the position of an atom, whereas internal coordinates use two atoms (A and B) to determine a bond distance, 3 atoms (A, B, and C) to describe a bond angle, and 4 atoms (A, B, C, and D) to describe a torsional (dihedral) angle. The LINK module of AMBER [17] was used to connect the seven glucose fragments together into the B-CD macrocycle. LINK connects the glucose residues in an arbitrary conformation, depending on the internal coordinates of the first three atoms of each residue. The EDIT module of AMBER then replaced each of

the atomic coordinates of the "dummy" glucose fragment with the appropriate coordinates from the B-CD X-ray crystal structure.

Since the X-ray crystal structure omitted hydrogen atoms, EDIT also assigned positions for the hydrogen atoms. The dihedral angles for the hydrogen atoms were assigned by EDIT by a calculation of the dihedral angles of all atoms bonded to the same atom as the hydrogen atom. For example, a hydrogen atom bonded to an oxygen atom that is bonded to a carbon-carbon connection would have a typical dihedral angle of approximately 70^{o}. The hydrogen atom was then placed in a chemically reasonable position by EDIT, as determined by the valency of the atom to which the hydrogen atom was attached. This procedure gave the starting structure of B-CD to be used in the next module of AMBER, PARM (parameterization)

The primary function of PARM is the assignment of parameters in the empirical energy function to the arrays (bond lengths, etc.) that have already been formed. This is accompanied by matching atomic symbols representing bonds, angles, and dihedrals to the type of the atoms comprising the bond, angle, and dihedral arrays. A distance of 2.0 A was selected as the cutoff for hydrogen-bond interactions. The PARM procedure gave the starting structure of the B-CD macrocycle used in the MINM (minimization) module of AMBER [17]. MINM adjusts the coordinates of a molecule with a modified conjugate gradient minimizer until the energy function is at a relative minimum.

The X-ray crystal structure of the B-CD macrocycle was modified, as described below, to accomodate the substituents for capped B-CD, as no X-ray crystal data was available for this molecule. The geometry of the N,N dimethyl formamide fragment was built from standard bond angles and bond lengths (including hydrogen atom positions) and was optimized with the MNDO (Modified Neglect of Diatomic Overlap) [21] method as implemented in the MOPAC program [22]. The X-ray coordinates of the glucose fragment, used in the above procedure for B-CD, were read into the graphics work area of Chem-X [18] using the "READ" command. The C9-C10 bond of this fragment (Figure 6) was then broken by the "MODIFY/CURSOR BREAK BOND" command of the Chem-X facility. The C10 fragment was then deleted from the graphics area by the "MODIFY/CURSOR KILL" command. The coordinates of the remaining fragment were then saved in the user area by the "WRITE PDB" command. The coordinates of the N,N-dimethyl formamide fragment were then read into the graphics work area of Chem-X. A hydrogen atom of one of the methyl carbons of the formamide fragment was deleted. This was done in order to facilitate connection of the formamide fragment to the glucose fragment. The coordinates of the modified glucose fragment (lacking the C10 substituent group) were then read into the graphics work area of Chem-X by the "READ/APPEND" command. This command allows the coordinates of more than one molecule to be read into the graphics work area at one time. Thus the glucose

fragment and formamide fragment could be simultaneously viewed on the screen of the graphics terminal. A bond of arbitrary length was then created between the C9 atom of the glucose structure and the methyl carbon atom, C15, of the formamide fragment in order to create the capped glucose fragment shown in Figure 13. This was faciliated by the "MODIFY/CURSOR MAKE BOND" command of the Chem-X software package. The bond length between the C9 atom of the glucose fragment and the C10 atom of the formamide fragment was set to a standard bond length of 1.497 A by the "MODIFY/CURSOR GEOMETRY" command. With the same command, the C9-C10-N11 bond angles was set to 109.5^{o}, while the C10-N11-C12 and C10-N11-C13 bond angles were set to 120.0^{o}. The file was then written out with the "WRITE FOREIGN" command, in a format compatible with the input format of GAUSSIAN 80 UCSF [23].

The capped glucose fragment was then used as input to GAUSSIAN 80 UCSF in order to determine "potential derived" atomic point charges (see Section C). This fragment provided "dummy" input coordinates and atomic point charges for the capped glucose fragment used in the PREP module of AMBER. The LINK module of AMBER was used to connect the seven capped glucose fragment together into the capped B-CD macrocycle. The EDIT module of AMBER replaced each of the glucose fragment coordinates with the appropriate coordinates from the X-ray structure. The dihedral angles for the atoms of the cap and the hydrogens were assigned by EDIT by the same procedure described previously for the

hydrogen atoms of the glucose fragment. This resulted in a starting structure with all the caps placed under the macrocycle to form an intrusive floor (Figure 14). This procedure gave the starting structure of capped B-CD used in the PARM and MINM modules of AMBER. As a result of the previous procedures, the B-CD and capped B-CD mimics differed by not only the number of atoms each contained, but also the number of atomic coordinates taken from X-ray crystal data, 77 for B-CD versus 70 for capped B-CD. The relevance of this point will be understood during analysis of the results (see Section IV B).

The numbering scheme used in the present study (Figures 6 and 13) to label atoms within a glucose fragment differs from that of the crystallographic scheme, as presented in Figure 15. The present scheme numbers the atoms sequentially from 1 through 98 for B-CD, and 1 through 112 for capped B-CD. In addition, the order of labeling is different in the two schemes. For example, C41 of the crystallographic scheme is not atom 4 of the present scheme, but rather C13 for the B-CD fragment, and C15 for the capped B-CD fragment. This can be seen by comparison of Figures 6, 13, and 15.

B. Force Field Parameters

The AMBER force field has been parameterized by Kollman and coworkers [24] to treat small molecules [25], proteins, and nucleic acids [24]; and by Venanzi and Bunce

[8,9], for cyclic urea mimics of alpha-chymotrypsin. Amber approximates the conformational energy of a molecule as the sum of bond stretching, angle bending, torsional, nonbonded, electrostatic, and hydrogen bond interactions. The potential energy function is generally given as a sum of strain energies and non-bonded interaction terms represented by:

$$
\begin{aligned}
E = & \sum_{\text{bonds}} K_r \left(r - r_{eq} \right)^2 \\
& + \sum_{\text{angles}} K_\theta \left(\theta - \theta_{eq} \right)^2 \\
& + \sum_{\text{dihedrals}} V_n \left[1 + \cos \left(n \phi - \gamma \right) \right] / 2 \\
& + \sum_{i<j} \left[A_{ij} / R_{ij}^{12} - B_{ij} / R_{ij}^{6} + q_i q_j / \left(\epsilon R_{ij} \right) \right] \\
& + \sum_{\text{H-bonds}} \left[C_{ij} / R_{ij}^{12} - D_{ij} / R_{ij}^{10} \right] \qquad (3)
\end{aligned}
$$

In Equation (3), K_r, K_θ, and V_n are bond stretching, angle bending, and torsional constants, respectively. The force field parameters are r_{eq} (the equilibrium bond length), θ_{eq} (the equilibrium bond angle), γ the torsional angle phase factor, A_{ij} and B_{ij} (the non-bonded parameters), and C_{ij} and D_{ij} (the hydrogen bond parameters). In equation (3), r represents the bond length, θ the bond angle, ϕ the dihedral angle, R_{ij} the distance between any two atoms i and j, q_i the charge on atom i, and ϵ the distance dependent

dielectric constant. ϵ is generally chosen as 1.0, but can be made distance dependent ($\epsilon = R_{ij}$) in order to simulate the effect of solvent. The distance dependent dielectric damps the effect of the long range interactions, thus increasing the percentage of short range interactions, and simulating the effect of polarization of the solvent molecule.

However, additional parameters were necessary to describe the cyclodextrin mimics of alpha-chymotrypsin. The parameters needed for B-CD and capped B-CD were for the OS-CH-OS angles (Figures 16 and 17). The CH atom type, as defined by AMBER, is an sp^3 carbon with one hydrogen, while the OS atom type is an sp^3 ester or ether oxygen. The AMBER parameter database contained bond angle parameters for a C2-CH-OS connection, where C2 is an sp^3 hybridized carbon with two hydrogens. An equilibrium bond angle value of 109.5° and an angle bending force constant of 80.0 Kcal mol^{-1} deg^{-2} were given in the AMBER database as the equilibrium angle bending parameters the C2-CH-OS environment. Since the hybridization state of the central carbon atom in the two systems is equivalent (i.e. both are sp^3 hybridized), the bond angle for the OS-CH-OS environment was chosen to be 109.5°, while the angle bending force constant was chosen as 80.0 Kcal mol^{-1} deg^{-2} .

The parameters needed for the capped B-CD were for the CH-C2-N and C2-N-C3 angles (Figure 17). The N atom type is an sp^2 hybridized nitrogen in an amide group. The database

contained parameters for a C2-C2-N connection. The equilibrium bond angle for C2-C2-N was given as 111.2°, while the angle bending force constant was given as 80.0 Kcal mol^{-1} deg^{-2} . These values were substituted for the CH-C2-N parameters since the central carbon atoms had the same hybridization state (i.e $C_{(sp^3)}$-$C_{(sp^2)}$- $N_{(sp^2)}$) and a similar chemical environment. The database contained angle bending parameters for CH-N-C3 connections, where C3 is an sp^3 hybridized carbon with three hydrogens. The equilibrium bond angle parameters for the CH-N-C3 were given as 118.0°, and 50.0 Kcal mol^{-1} deg^{-2} for the bond angle and angle bending force constants, respectively. These values were substituted for the C2-N-C3 parameters, by approximating the chemical environment of C2-N-C3 to that of CH-N-C3.

C. Atomic Point Charges

The atomic point charges for the B-CD and capped B-CD molecules were obtained by separate quantum mechanical calculations on a representative glucose and capped glucose fragment, respectively. The "potential derived" atomic point charges obtained for the glucose fragment were then assigned to the other six glucose fragments in the B-CD macrocycle. In a similar manner, the point charges obtained for the capped glucose fragment were assigned to the other six capped glucose fragments in the capped B-CD macrocycle.

The structures used as input to the atomic point charge calculation were: (1) The X-ray crystal structure of the selected glucose fragment from the B-CD macrocycle;

and (2) The capped glucose fragment built from the X-ray structure of the glucose fragment combined with the MNDO-optimized N,N-dimethyl formamide fragment, as described in Section A of Methods.

Since the united atom AMBER force field was to to be used for the conformational analysis, the hydrogen atoms were removed from the carbon atoms of the glucose and capped glucose fragments. In the united atom (UA) approximation, the hydrogen atoms on aliphatic and aromatic carbons are not treated explicitly. The force field parameters and atomic point charges are then derived for each group (such as $-CH_3$) as a unit. The calculations were carried out in the STO-3G basis set with the GAUSSIAN 80 UCSF [23] software package. The atomic point charges were calculated in the united atom approximation (UA) for both of the molecular fragments: the glucose and capped glucose fragments. In this procedure, the charges on the heavy (non-hydrogen) atoms were fit in order to effectively reproduce the electrostatic potential calculated on the surface of the molecule. The charges approximated in this fashion are known as "potential derived" point charges [26].

The STO-3G basis set for any first row atom (i.e. carbon, oxygen, and nitrogen) consists of only 2 shells. A shell is a set of basis functions (ϕ_μ) with shared exponents. An s-shell contains a single s-type basis function, while an sp-shell contains four basis functions with common gaussian exponents: one s-type function and

three p-functions p_x, p_y, and p_z. The first is an s-shell consisting of a set of 3 primitive gaussian functions least squares fitted to a Slater 1s orbital with an appropriate scale factor. The other is an sp-shell that is a least squares fit of 3 gaussians to Slater 2s and 2p orbitals with the constraint that the s and p functions have equal exponents [23].

D. Effect of Scaling Parameters

AMBER was used to perform a scaling study on B-CD and capped B-CD in order to determine the sensitivity of the 1-4 non-bonded terms to modification. An example of a 1-4 interaction, which is a non-bonded type interaction, is presented in Figure 18. The 1-4 van der Waals term of the force field is approximated by Equation (4A), while the 1-4 electrostatic component is approximated by Equation (4B).

$$\text{1-4 NB Term} = (\text{NB})^{-1} \sum_{\text{1-4 non-bonded terms}} [A_{ij} / R_{ij}^{12} - B_{ij} / R_{ij}^{6}] \quad (4A)$$

$$\text{1-4 EEL Term} = (\text{EEL})^{-1} \sum_{\text{1-4 non-bonded terms}} [Q_i Q_j / (R_{ij}^{10})] \quad (4B)$$

As can be seen from Equations (4A) and (4B), the van der Waals and electrostatic contributions to the force field are inversely related to the 1-4 scaling parameters, NB and EEL.

The NB and EEL parameters were scaled from 0.5 through 3.0, respectively. Thus for constant NB (i.e. at a value of 0.5), the value of EEL was varied from 0.5 to 3.0. An analagous procedure was followed for constant EEL with NB following the same range.

E. Structural Superposition

In order to investigate the effect of energy minimization and scaling of the 1-4 non-bonded and 1-4 electrostatic terms, each energy minimized mimic was fitted to the X-ray crystal macrocycle using the RMS module of AMBER updated by Weiner [27]. The RMS (root mean square) program compares the coordinates of two systems by moving the coordinates of system 2 to minimize the rms deviation with the coordinates of system 1.

Prior to using the RMS package, the X-ray crystal structure was moved into the optimal orientation by using the "SET VIEW/PLANE" and "MODIFY" commands of Chemgraf/Chem-X [18]. The glycosidic linking oxygens (indicated in Figure 19) were used to define an x-y plane at z=0. This was accomplished by fitting the "best plane" through the coordinates of the glycosidic oxygens with the "SET VIEW/PLANE" command. This placed the glycosidic oxygens in an x-y (z = arbitrary) plane. The arithmetic average value of the z-coordinate of the seven glycosidic oxygens was then determined. The atom with the z-coordinate closest to the the calculated average was chosen as the average oxygen. The macrocycle was then translated along the z-axis so that

this glycosidic oxygen was at z = 0. Since the screen of the graphics terminal corresponds to the x-y plane, this orientation allows the viewer to "look down into" the macrocycle. Superposition of a calculated structure upon the X-ray structure, oriented in this fashion, clearly points out deviations in atomic positions.

Once the X-ray structure of the B-CD was in this orientation, each minimized structure was fit to it by an RMS fitting of all atoms except hydrogens for B-CD, and all atoms except hydrogens and caps for capped B-CD. Deviation in atomic positions of the superimposed structures gave an estimate of conformational change upon energy minimization. It also indicated how addition of the caps might affect the conformation of the macrocycle. The change in conformation of the macrocycle is of interest since the caps are believed to form an intrusive floor [4] at the bottom of the macrocycle. Thus, the magnitude of the deviations of the fitted atoms from the mean can give a qualitative indication of the effect of the addition of the caps on the conformation of the macrocycle.

The deviations of most interest are those of O3 and O6 for B-CD and capped B-CD, respectively (Figures 7 and 20). These are the secondary hydroxyl groups that are found on the top rim of the macrocycle. These are important since they are the hydroxyl groups that can potentially mimic the action of the hydroxyl group of Ser-195 of alpha-chymotrypsin in acyl transfer to the substrate.

F. Molecular Electrostatic Potential

The general electrostatic recognition pattern of the biomimetic catalyst for a substrate was investigated by the use of molecular electrostatic potential contour maps. The molecular electrostatic potential is a physical observable [11], measured by X-ray diffraction and scattering experiments. The potential can be generally described by the following equation:

$$V_{(\underset{\sim}{r})} = \sum_{\text{nuclei A}} (Z_A / | \underset{\sim}{R}_A - \underset{\sim}{r} |) - \int \rho_{(\underset{\sim}{r}')} \, d\underset{\sim}{r}' / | \underset{\sim}{r}' - \underset{\sim}{r} | \qquad (5)$$

where $V_{(\underset{\sim}{r})}$ is the electrostatic potential of the molecule at point $\underset{\sim}{r}$, Z_A is the charge on nucleus A located at $\underset{\sim}{R}_A$, and $\rho_{(\underset{\sim}{r}')}$ is the electron density distribution derived from the quantum mechanical wave function. Since the calculation of the wave function is beyond the range of the central processing unit memory and disk storage space of present supercomputers, it is desirable to approximate Equation (5). The electrostatic interaction of a positive point charge with a static charge distribution of the molecule, modeled by point charges placed at the positions of the atomic nuclei, can be approximated by the following equation:

$$V(\underset{\sim}{r}) = \sum_{\text{nuclei A}} \left(Q_A / \left| \vec{R}_A - \vec{r} \right| \right) \qquad (6)$$

where Q_A is the atomic point charge described in Section C. Since the potential derived point charges are fit to reproduce the molecular electrostatic potential, they approximate the electrostatic and nuclear contributions of the atoms.

The molecular electrostatic potential contour maps were calculated for the orientations of the fitted structures as described in Section E. The molecular electrostatic contour maps were represented by 2-dimensional electrostatic potential maps. The 2-dimensional maps were calculated using the "SET DUMMY" and "SET MAP" facilities of Chem-X [18]. The "SET MAP" command calculates the 2-dimensional electrostatic potential map in the x-y plane at the z-coordinate of a chosen atom. In order to faciliate the calculation of the map at different values of z, a dummy atom was defined. This atom could then be translated up and down the z-axis and the electrostatic potential calculated at each chosen z-value of the dummy atom.

The "SET DUMMY" command calculates the coordinates of the centroid (dummy atom) as the average x, y, and z-coordinates of a chosen list of atoms; in this case, the glycosidic oxygens (Figure 19). For example, for a B-CD macrocycle fit to the X-ray structure as described in Section E, the z-coordinate of the centroid would be approximately zero. Alternative positions for the centroid

were obtained by the "MODIFY/GEOMETRY ATOM NAME" command. The z-coordinates were changed from z = 0 A through z = 6 A, and z = 0 A through z = -6 A by increments of 2 A. The z-axis was chosen as the direction to manipulate the centroid since the screen of the graphics terminal is defined as the x-y plane by the molecular display software.

The "SET MAP/CONTOUR" command gives user-defined contour energy levels in units of Kcal/mole. Points of equal energy are connected, thus forming a qualitative picture of the molecular electrostatic potential of the mimic. Thus, the centroid could be used to yield qualitative maps above and below the mimic by simple manipulation of its z-coordinate. Therefore, the electrostatic potential contour maps can give a qualitative indication of the long-range electrostatic potential pattern that the mimic displays for the substrate.

III. RESULTS

A. Energy Minimization

The results of the energy minimization of the B-CD and capped B-CD mimics of alpha-chymotrypsin are presented in Tables I and II, respectively. The minimization was performed by the AMBER software package [17]. AMBER decomposes the total energy (T.E.) into bond stretching (BOND), bond angle bending (B.A.), dihedral (DIH.), van der Waals (VDW), electrostatic (ELEC), 1-4 van der Waals (1-4 VDW), hydrogen bonded (H-B), and 1-4 electrostatic (1-4 EEL) energy contributions. The minimization was performed as a function of 1-4 van der Waals and 1-4 electrostatic scaling parameters, NB and EEL, respectively. Tables IA and IIA present the results to highlight the changes in energy with NB for constant EEL. Tables IB and IIB present the results of Tables IA and IIA, respectively, reorganized to show the changes in energy with EEL for constant NB.

Column 1 of each table shows an alphabetical letter as a function of NB and EEL. These names are in no set order and are only used to help distinguish the different input sets. The total energy from the minimization calculation is presented in column 2. The bond stretching, angle bending, van der Waals, electrostatic, hydrogen bonding, 1-4 van der Waals, and 1-4 electrostatic components of the minimized energy are shown in columns 3 through 9, respectively. Columns 10 and 11 contain the 1-4 NB and 1-4 EEL scaling parameters, respectively.

The minimized total and component energies for B-CD, at

constant EEL and varying NB, are given in Table IA; the energies at constant NB and varying EEL are given in Table IB. Several trends are observed. For constant EEL, the 1-4 van der Waals term decreases with increasing NB. This is because the term varies inversely with the NB scaling parameter, as shown by Equation (4A). Also for increasing EEL at constant NB, the 1-4 EEL term decreases because of Equation (4B). This can be seen clearly from Table IB.

Although the bond stretching, bond angle bending, dihedral, van der Waals, electrostatic, and hydrogen bonded terms are not explicitly dependent upon the scale factors, some trends are observed. The dihedral and van der Waals terms are essentially independent of variation in NB and EEL. For constant EEL, the electrostatic contribution slightly increases in absolute magnitude (becomes more negative) with increasing NB parameter. For constant EEL in the range of 1.0 to 2.0, the bond angle component decreases with increasing NB. The bond stretching contribution decreases with increasing NB for constant EEL in the range of 0.5-3.0. The hydrogen bond term increases in magnitude (but becomes more negative) with NB for constant EEL (Table IA), and increases significantly in magnitude with EEL for constant NB (Table IB). The total energy follows the trend of the electrostatic and 1-4 electrostatic components, since they are the largest contributors (in magnitude) to the total energy. As a consequence, the total energy decreases with increasing EEL.

A general comparison of Tables IA and IB indicates that the total and component energies share a common trend. There is a decrease in total energy, bond energy, and electrostatic energy with increase in scaling factors NB or EEL. In addition, comparison of the total energies within a particular group of constant NB or constant EEL indicates that total energy varies to a greater degree with change in EEL than with change in NB.

The variation of the conformational energy of capped B-CD, with scaling factors EEL and NB, is given in Tables IIA and IIB, respectively. The same general trends observed for the various energies of B-CD are also found in Tables IIA and IIB.

A direct comparison of the energies for B-CD and capped B-CD indicates that the van der Waals component of the total energy is significantly lower in value (but larger in absolute magnitude) for capped B-CD than for B-CD. The opposite is true of the 1-4 van der Waals term. The bond stretching, bond angle bending, dihedral angle, and hydrogen bond energies, however, are of approximately the same order of magnitude for both mimics. This trend is expected since the addition of the "cap" substituent to the cyclodextrin macrocycle provides the potential for additional van der Waals interactions.

B. Hydrogen-Bond Interactions

AMBER identifies atoms that could potentially form hydrogen bonds, based on a user specified-cutoff

parameter. The cutoff distance used in this study was 2.0 A. Six pairs of intramolecular hydrogen-bonded atoms were found for B-CD and capped B-CD, respectively, using scaling factors NB = 1.0 and EEL = 1.0. The hydrogen bonds formed were between the secondary hydroxyls. For example, the hydrogen atom H4 of oxygen O3 was hydrogen bonded to the oxygen O6 of an adjacent fragment. The hydrogen-bonded atoms, called atoms 1 and 2 in the Tables, along with the bond distances are presented in Tables IIIA and IIIB for B-CD and capped B-CD, respectively. Column 1 of the tables gives the hydrogen atom (called Atom 1) that initiates the hydrogen bond, while column 2 gives the fragment number of that hydrogen. Column 3 gives the oxygen atom (called Atom 2) involved in the hydrogen bond with atom 1, while column 4 gives the fragment number of atom 2. Column 5 gives the hydrogen bonding distance between the two atoms. The hydrogen bond distances ranged from 1.77 A (column 5) for the hydrogen bond between H4 (column 1) of fragment 1 (column 2) and O6 (column 3) of fragment 7 (column 4), to 1.99 A (column 5) for H4 of fragments 4 and 5 (column 2) and O6 (column 3) of fragments 5 and 6, respectively.

The sequence of the hydrogen bonds is for the hydrogen of the oxygen in position 3 of each fragment to hydrogen bond to the oxygen in position 6 of an adjacent fragment. Thus, the sequence for the hydrogen bonded fragments is as follows: Hydrogen 4 of fragment 1 is hydrogen bonded to oxygen 6 of fragment 7; Hydrogen 4 of fragment 2 is

hydrogen bonded to oxygen 6 of fragment 3; Hydrogen 4 of fragment 3 is hydrogen bonded to oxygen 6 of fragment 4; Hydrogen 4 of fragment 4 is hydrogen bonded oxygen 6 of fragment 5; Hydrogen 4 of fragment 5 is hydrogen bonded oxygen 6 to fragment 6; and Hydrogen 4 of fragment 6 is hydrogen bonded to oxygen 6 of fragment 7.

All distances are well within the experimental distance of 2 A suggested for the formation of a hydrogen bond [28]. Experimental X-ray [29] and molecular dynamics simulations [30] evidence also suggests the existence of this hydrogen bonded network in alpha-cyclodextrin. The X-ray hydrogen bond distances for alpha-cyclodextrin ranged from 1.67 A to 1.95 A [29]; while the hydrogen bond distances obtained from the simulations for alpha-cyclodextrin ranged from 1.70 A to 2.21 A [30].

C. RMS Deviations

The RMS (Root Mean Square) module of AMBER [17,27] was used to compare the deviation in atomic positions of B-CD or capped B-CD when the calculated structures were separately fit to the X-ray structure of B-CD. The atomic positions compared were those of the heavy (non-hydrogen) atoms within the macrocycle. This was done for three reasons: (1) Since the X-ray structure of B-CD did not show hydrogen atom positions, there was no reason to include hydrogen atoms in the fit; (2) There was no X-ray structure of the capped B-CD compound available, so the atoms of the "cap" substituents were not included in the fit; and (3)

The goal of this research is to study the effect of addition of the "caps" on the orientation of the potential nucleophiles (the secondary hydroxyl oxygens around the rim of the macrocycle). For this reason, the change in orientation of the heavy atoms of the macrocycle (especially the secondary hydroxyl oxygens) caused by addition of the caps is of importance. As a result, 77 atoms were compared for B-CD (i.e. all atoms excluding hydrogens), whereas 70 atoms were compared for capped B-CD (i.e. all atoms excluding hydrogens and those atoms of the caps). The difference in the number of compared atoms for B-CD and capped B-CD resulted from the O11 substituent of the B-CD macrocycle being replaced by the N11 atom of the cap on each of the seven capped B-CD fragments (Figure 13).

The RMS mean and standard deviations of the fit of B-CD to the X-ray structure of B-CD are presented in Tables IVA and IVB. Table IVA is arranged to show the trends as the scaling factor NB is varied from 0.5 to 3.0 for constant EEL, whereas Table IVB contains the same data arranged to show the trends as EEL is varied for constant NB. Column 1 of each table shows a file name with an alphabetical letter as a function of NB and EEL. These names are in no set order and are only used to help distinguish the different input sets. The total energy from the minimization calculation is presented in column 2. Column 3 shows the rms deviation for the 77 heavy atoms of the macrocycle that were chosen for the fit; whereas column

4 shows the rms deviation for all 98 atoms (including hydrogens). The mean and standard deviations, based on all 98 atoms, are presented in columns 5 and 6, respectively. In addition, column 8 identifies the atom whose position has the maximum deviation from the mean. This deviation is given in column 7. The scaling parameters, NB and EEL, are presented in columns 9 and 10.

As can be seen from column 7, the RMS deviation for the 77 atoms ranges from 0.23 A to 0.73 A, depending on the value of the scaling parameters. It should be noted that the calculated structure is compared to the X-ray structure of the B-CD that was complexed with a 1,4-diazabicyclo(2.2.2.)octane clathrate. From the fit of all atoms (column 4), it is worthwhile noting that except for one case, the atoms with the maximum deviations (column 8) are hydrogens. This is not unexpected because the all-atom comparison matches the hydrogen atom positions assigned by the EDIT module of AMBER to the minimized hydrogen atom positions. Although EDIT adds hydrogens at standard bond lengths, bond angles, and dihedral angles, these positions are not necessarily the optimized positions. The exception in column 8 occurs for oxygen atom 39 (a primary oxygen), which is situated at the "bottom" of the macrocycle, and does not potentially mimic the hydroxyl oxygen of Ser-195 (Figure 7). Thus, as a consequence, the magnitude of its deviation may be unimportant to the catalytic process.

Table VA shows statistical deviations for the fit of capped B-CD to the X-ray structure of B-CD. Table VA

arranges the data as a function of NB, while Table VB shows the same data as a function of EEL. The deviations for the 70 fitted atoms (column 3) of the macrocycle range from 0.5029 A to 0.8170 A. The lowest deviation occurs at NB = 2.0 and EEL = 1.5 for the 70 atoms. From the fit of all atoms (column 4), it can be seen that the maximum deviation (column 7) from the mean occurs for either atoms O14, O62, or O110. All these atoms are found in the caps. Again, this is not unexpected because the all-atom fit essentially compares the starting structure of the capped B-CD (as assigned by EDIT) to a minimized structure.

A general comparison of the results of Tables IV and V indicates that the rms deviations are lower for B-CD than for capped B-CD. Although the comparisons are for a different number of atoms (77 for B-CD versus 70 for capped B-CD), the rms deviations indicate the effect that addition of the caps has on the conformation of the B-CD macrocycle. The rms data shows that the addition of caps changes the structure of the macrocycle from that shown in the X-ray structure [19].

Oxygens number O3 and O6 within a glucose fragment (Figure 6 and Figure 7) can potentially mimic the action of the hydroxyl oxygen on Ser-195 because they are positioned around the rim of the macrocycle. The distance difference in the calculated positions compared to the X-ray position of oxygens O3 and O6 of B-CD are presented in Tables VIA and VIB, respectively. The differences are shown

for NB = 1.0 and a range of EEL from 0.5 to 3.0. Column 1 of each Table gives the fragment number of the O3 or O6 atom in the B-CD and capped B-CD macrocycles, respectively. Columns 2 through 5 give the atomic position distance differences as a function of EEL scaling parameter.

For oxygen atom O3 of the B-CD macrocycle at EEL = 0.5, the distance difference ranged from 0.093 A for fragment number 5 to 0.756 A for fragment number 1. For EEL = 1.0, the distance difference ranged from 0.127 for fragment number 2 to 0.360 for fragment number 6. For EEL = 1.5, the distance difference ranged from 0.157 A for fragment number 5 to 0.693 A for fragment number 3. For EEL = 2.0, the distance difference ranged from 0.139 A for fragment number 4 to 0.445 A for fragment number 3. For EEL = 3.0, the distance difference ranged from 0.172 A for fragment number 5 to 1.342 for fragment number 3. Table VIA indicates that for a given EEL, there is a range of O3 position differences exhibited by the fragments. That is, not every fragment behaves identically upon minimization. In addition, for a given fragment, the O3 atomic difference position depends on the value of EEL. This indicates that the optimized position of O3 is sensitive to the scaling of the 1-4 EEL parameter.

Table VIB gives the atomic position difference for oxygen atom O6 at NB = 1.0, and a range of EEL from 0.5 through 3.0. At EEL = 0.5, the position differences ranged from 0.307 A for fragment number 4 to 0.817 A for fragment number 5. At EEL = 1.0, the distance difference ranged from

0.056 A for fragment number 4 to 0.329 A for fragment number 6. At EEL = 1.5, the distance difference ranged from 0.108 A for fragment number 1 to 0.794 A for fragment number 3. At EEL = 2.0, the distance difference ranged from 0.032 A for fragment number 1 to 0.595 for fragment number 7. Finally, at EEL = 3.0, the value of the difference ranged from 0.195 A for fragment number 1 to 1.566 A for fragment number 3. From this it can be seen that oxygen atom O6 position is also sensitive to scaling of the 1-4 EEL term.

Evaluation of Tables VIA and VIB shows that, for a particular value of EEL, the difference between the calculated and X-ray oxygen positions is not significantly different for either O3 or O6 in B-CD. Thus, the magnitude of these results supports the choice of angle bending parameters used (see Section A of Methods) for the B-CD fragment (Figure 16). This result is significant because the same parameters were used for the capped B-CD macrocycle.

The atomic position distance difference for oxygens O3 and O6 of capped B-CD for same NB value and the range of EEL values previously described are presented in Tables VIIA and VIIB, respectively. For oxygen atom O3 at EEL = 0.5, the distance difference ranged from 0.0489 A for fragment number 5 to 1.3899 A for fragment number 1. For EEL = 1.0, the distance difference ranged from 0.2509 A for fragment number 3 to 2.3272 A for fragment number 4. For EEL = 1.5, the values of the distance difference ranged from 0.1112 A

for fragment number 3 to 2.1553 A for fragment number 4. For EEL = 2.0, the deviations ranged 0.2093 A for fragment number 3 to 2.0109 A for fragment number 4. For EEL = 3.0, the deviations ranged from 0.3100 A for fragment number 3 to 2.0657 A for fragment number 4. Table VIIA indicates that the maximum difference in the O3 position for capped B-CD occurs for fragment 4, except at EEL = 0.5. Since the difference in the O3 position of capped B-CD is seen to depend in general on EEL, the results of Table VIIA agree with Table VIA in that the O3 position is sensitive to the scaling of the 1-4 EEL term.

Table VIIB shows that for oxygen O6 at EEL = 0.5, the differences ranged from 0.3907 A for fragment number 6 to 1.4352 A for fragment number 1. For EEL = 1.0, the distance difference ranged from 0.1965 A for fragment number 3 to 2.2394 A for fragment number 4. For EEL = 1.5, the values ranged from 0.1673 A for fragment number 3 to 2.0241 A for fragment number 4. For EEL = 2.0, values of the distance difference varied from 0.1917 A for fragment number 1 to 1.9822 A for fragment number 4. For EEL =3.0, values ranged from 0.2534 A for fragment number 1 to 1.9692 for fragment number 4. Table VIIB indicates that the maximum difference in the O6 position of capped B-CD occurs for fragment 4, except at EEL = 0.5. This is in agreement with Table VIIA which showed that the maximum O3 difference also occured for fragment 4. This seems to indicate that the cap substituent causes a noticeable change in the orientation of the secondary hydroxyls of fragment 4. Although significant

deviations (greater than 0.7 A) in atomic position differences are seen in other fragments, there is not such a distinctive independence of EEL as exhibited by fragment 4. For example, at EEL = 1.0, fragments 1, 4, and 6 show large differences for the O3 position in the calculated macrocycle to the X-ray structure of capped B-CD (Table VIIA). However, at EEL = 1.5, fragments 4, 6, and 7 show large O3 position differences. Nevertheless, it is clear from Tables VIIA and VIIB that the addition of the caps causes a change in the orientation of the secondary hydroxyl oxygens of some of the glucose fragments of the macrocycle.

Comparison of the O3 and O6 position differences in Tables VI and VII shows that the differences are consistently larger in capped B-CD than in B-CD. This can be seen in Figure 21 which compares the minimized structure of capped B-CD (NB = 1, EEL = 1) to that of the X-ray structure. This figure is a visual display of the data in column 3 of the Tables VIIA and VIIB. It can be seen from Figure 21 that in fragments 1 and 4, the caps move out (away from under the macrocycle) causing the secondary hydroxyls to move in (towards the center of the cavity). In fragment 6, the secondary hydroxyls move out, while the cap moves in, forming an intrusive floor. Figure 21 shows that in fragments 2, 3, 5, and 7, the glucose fragment of capped B-CD almost exactly superimposes on that of the X-ray structure. This is supported by the data in Table VII which shows that the smallest difference in the O3 and the O6

position occur for these fragments. The relationship of the structure of the capped B-CD to its catalytic function will be commented on in the Discussion Section.

D. Molecular Recognition by Electrostatic Complementarity

The general electrostatic recognition pattern of the biomimetic catalysts was investigated by analysis of two dimensional molecular electrostatic potential contour maps of B-CD and capped B-CD. The two dimensional maps presented are approximations of the electrostatic potential, for reasons previously given in Section F of the Methods. The maps correspond to scaling factors NB and EEL equal to one. The mimics were oriented in the x-y plane using the glycosidic linking oxygens (Figure 19) as described in Section E of Methods.

The atomic point charges used in the calculation of the maps are given in Table VIII. Column 1 gives the atoms in the glucose and capped glucose fragments. Column 2 gives the charges for each atom of the glucose fragment; whereas column 3 gives the charges for each atom of the capped glucose fragment. Comparison of the charges in columns 2 and 3 shows the effect of the addition of the caps on the charges of the atoms of the glucose fragment. As can be seen from column 3, the atomic point charges for the 14 atoms of the glucose fragment range from -0.5852 for atom O6 to 0.4826 for atom C5. The atomic point charges for the capped glucose fragment range from -0.5605 for atom O6 to

0.5029 for atom C5. Therefore, in both fragments, C5 has the largest point charge and O6, the smallest. In fact, the first 10 sets of point charges (C1 through C10) are very similar for both fragments. Only at the point of attachment of the cap (C13 through O14), do the point charges differ significantly. This is reasonable since the electrostatic field (to which point charges are fit) would be expected to be different in the region of a cap substituent as compared to a hydroxyl group. This also tends to indicate that assigning the charges of the entire B-CD molecule from charges derived from a quantum mechanical calculation on one glucose fragment is a reasonable approximation. The results seem to indicate that similar point charges would have resulted had we used a "double" glucose fragment (2 linked glucose molecules) to calculate the charges.

Two dimensional electrostatic potential maps were obtained in the x-y (z = 0) plane, and the positive and negative z-directions. The electrostatic potential contour maps, taken at increments in the z-coordinate of the centroid, allow a qualitative determination of the electrostatic potential pattern presented to the substrate as it approaches the mimic.

The electrostatic potential contour maps for B-CD and capped B-CD are presented in Figures 22 through 35, as a function of the z-coordinates of the centroid. The contour levels chosen for display are the same in each figure. The energy (in units of kcal/mole) is represented

by contour levels at: -50, -30, -10, 0, 10, 30, and 50. The values of the contour levels are written directly on the maps, adjacent to the respective contour line. Lines of equal energy are connected on the maps. Thus the reader is asked to follow the enumerated lines to get a qualitative view of the map.

The molecular electrostatic potential contour maps for B-CD are presented in Figures 22 through 28. The molecule is oriented with the glycosidic oxygens (Figure 19) in the x-y plane at approximately z = 0 A. The secondary oxygens (O3,O6) of each fragment are found along the negative z-direction, while the primary hydroxyl (O11) of each fragment is found along the positive z-direction. The general characteristics of the maps are as follows. The potential of the macrocyclic cavity appears to be very positive and symmetrical, at z = 0 A, in the plane within the cavity. At z = 2.0 A, near the bottom of the cavity where the primary hydroxyls are to be found, the map changes slightly, becoming less positive in the region external to the cavity due to the lone pairs of the oxygens. From a distance of z = 4.0 A, the cavity appears even less positive, although still symmetric. At z = 6.0 A, approximately half of the cavity appears positive, while the other portion is essentially neutral because the map is calculated in a plane far from the lone pairs of the primary hydroxyl oxygen atoms.

As expected, since the molecule is not symmetric with respect to reflection through the x-y (z = 0) plane, the

maps are different in the negative z-direction. At z = -2.0 A, near the secondary hydroxyls on the rim of the cavity, the appearance of the map is essentially the same as at z = 0 A, as indicated by the energy levels. The map is still essentially positive at z = -4.0 A. However, the positive appearance has greatly diminished when compared to the maps at z = 0 A, and z = 2 A. At z = -6.0 A, the entire cavity of the macrocycle appears neutral as indicated by the energy level.

Comparing the maps along the positive z-direction, (Figures 23 through 25) to the maps along the negative z-direction (Figures 26 through 28), it can be seen for the same z-increment, the maps along the positive z-direction tend to appear more positive than along the negative z-direction. It is expected that the contribution of the secondary hydroxyl oxygens to the electrostatic potential along the negative z-direction would be greater (in magnitude) than that of the primary oxygens along the positive z-direction, since the number of secondary oxygens are twice as many as primary oxygens. Therefore the electron density of the lone pair of 2 neighbouring oxygens show up as negative segments on the map. Thus, the maps give not only a qualitative indication of the complementary electrostatic pattern that the substrate must present to the mimic, but also give an approximation of the incremental changes in the electrostatic interactions experienced by a substrate approaching from the "top" and "bottom" of the

macrocycle.

The molecular electrostatic potential contour maps for capped B-CD are presented in Figures 29 through 35. The molecule is oriented with the glycosidic oxygens (Figure 19) in the x-y plane at approximately z = 0 A. The secondary hydroxyls (O3, O6) of each fragment are found along the negative z-direction, while the caps are found along the positive z-direction. At z = 0 A, in the plane within the cavity, the potential of the macrocyclic cavity appears to be very positive and symmetrical. At z = 2 A, the map changes slightly, becoming less positive. From a distance of z = 4 A, near the bottom of the cavity and near the nitrogen atoms of the caps, the cavity still appears positive. However, the positive appearance has greatly diminished when compared to the maps at z = 0 A and z = 2 A. The change in the map is due to the fact that the map is calculated in a plane close to the lone pairs of the nitrogens of the caps. From a distance of z = 6 A, near the bottom of the cavity with the carbonyl oxygen atoms, the entire cavity appears negative due to the high electron density around the carbonyl oxygens of the caps.

As expected, since the macrocycle is non-symmetric with respect to reflection through the x-y (z = 0) plane, the maps are different in the negative z-direction. At z = -2 A, near the secondary hydroxyls on the rim of the cavity (Figure 20), the appearance of the map is essentially the same as at z = 0 A. From a distance of z = -4 A, the cavity appears positive, though much diminished when

compared to the maps of the cavity at z = 0 A, and z = -2 A. From a distance of 6 A, the appearance of the cavity is still positive. However, as indicated by the energy levels on the map, there is a significant decrease in positive appearance.

Comparing the maps along the positive z-direction, (Figures 30 through 32) to the maps along the negative z-direction (Figures 33 through 35), it can be seen for the same z-increment, the maps along the negative z-direction tend to appear more positive than along the positive z-direction. This is due to the fact that the caps are found along the positive z-direction. The nitrogen atoms of the caps are all oriented around z = 4 A, while the carbonyl oxygen atoms of the caps are oriented around z = 6 A. Therefore, it is expected that the contribution of the carbonyl oxygen to the electrostatic potential along the positive z-direction would be greater than that of the secondary oxygens along the negative z-direction, since the carbonyl oxygen is double bonded to the carbonyl carbon. The electrons of the carbonyl double bond hold together atoms of quite different electronegativety, and hence the electrons are not equally shared; in particular, the mobile pi electron cloud is pulled strongly toward the more electronegative atom, oxygen [31]. In addition, the lone pairs of the nitrogen and carbonyl oxygens of the caps increase the electron density around z = 4 A and z = 6 A, thus also contributing to the negative regions shown on

the maps.

Comparing the general characteristics of the maps for B-CD and capped B-CD at z = 0 A, it can be seen that the maps are very similar with the capped B-CD showing larger regions of positive potential (Figures 22 and 29). The maps for B-CD and capped B-CD at z = 2 A, along the primary hydroxyls of B-CD, are essentially the same, except that the maps for capped B-CD show larger areas of positive potential (Figures 23 and 30). The maps for B-CD and capped B-CD at z = 4 A, along the nitrogen atoms of the caps of capped B-CD, again are essentially the same, except the maps for B-CD show larger areas of positive potentials. The maps for B-CD and capped B-CD at z = 6 A, along the carbonyl oxygen atoms of capped B-CD, differ significantly (Figures 25 and 32). The map for B-CD appears positive, while the map for capped B-CD appears essentially negative. These results are expected since the hydroxyl oxygen at the O11 position of a glucose fragment was replaced by a cap substituent, which contained a carbonyl oxygen and a nitrogen. The effect of the nitrogen atoms and carbonyl oxygen atoms on the map of the capped B-CD macrocycle was explained previously.

The contour maps of B-CD and capped B-CD are very similar for z = -2.0 A to z = -6.0 A (Figures 27-29 and 33-35). The caps in B-CD "move" the secondary oxygens closer to the rim of the cavity of the macrocycle. Thus, the effect of the lone pairs of the secondary oxygens on the map of the B-CD macrocycle is seen at distances closer than

4A. The fact that the maps are still similar is not unexpected because the addition of the caps to the macrocycle of B-CD resulted in the replacement of the primary oxygens along the positive z-direction with caps (along the positive z-direction). The comparison of the maps for B-CD and capped B-CD suggests that the caps affect the conformational properties of the B-CD macrocycle, but do not significantly alter the electrostatic recognition pattern presented to a substrate, except in the region of the caps. Since the substrate would approach the cavity from the "top" of the macrocycle (on the side of the macrocycle opposite to the caps), this difference does not affect the overall electrostatic recognition pattern presented by the mimic to a substrate.

IV. DISCUSSION

As explained in the Introduction, the primary goal of the present work was to investigate the effect of "capping" on the conformation of the B-CD macrocycle. The conformational and molecular electrostatic recognition properties of B-CD and capped B-CD were studied using the computational procedure described in the Methods Section.

A. Test of Force Field Parameters

An important test of any force field, is its ability to reproduce experimental data. The formation of intramolecular hydrogen bonds (Tables IIIA and IIIB) between H4 of one fragment and O6 of an adjacent fragment seem to reproduce the experimental X-ray data [29], as well as the results of computer simulations [30]. In addition, the RMS statistical data (Tables IVA and IVB) indicates that the minimization procedure does not significantly alter the coordinates of the B-CD macrocycle when compared to the X-ray structure. Thus, the force field seems to reproduce experimental structural (X-ray) data and the environment (hydrogen bonds).

These results are important because the same angle bending parameters were used for capped B-CD (Figure 19). In addition, these results seem to lend credence to our reasoning used for the estimation of the missing angle bending parameters from the AMBER database; that is, to use equivalent hybridization states to estimate equilibrium bond angles and bond stretching force constants.

B. Effect of Caps on Conformation

As explained in Section D of the Introduction, cyclodextrins in their native form show many features characteristic of enzymes: (1) specificity; (2) the formation of catalyst-substrate complexes prior to chemical transformation; and (3) large rate accelerations. However, the rate accelerations resulting from a substrate binding into the cavity of the cyclodextrin are quite modest. Thus, this provided the impetus to either alter the molecular architecture of cyclodextrin or design substrates that provided larger acceleration gains.

Breslow [4] added caps to the B-CD macrocycle in order to alter the geometry of the cyclodextrin cavity. This change, as suggested by Breslow, increases the rate of the pseudo-first order reaction from approximately 10^2 in B-CD to values of 10^6 or better. This rate change was expected by Breslow since the change in the dimensions of the cavity that resulted from capping brings the complex closer to the geometry of the transition state.

The present work added the cap to the glucose fragment as described in Section A of the Methods. The EDIT-generated capped B-CD, when read into the graphics work area of Chem-X, showed all the caps forming an intrusive floor under the macrocycle. Upon minimization, some of the caps "moved" from under the cavity. The intrusive floor was still preserved, however, but not by all of the caps. This

result seems to yield two findings: (1) The steric energy is too great for all the caps to be under the cavity (i.e. there is too much steric hindrance); and (2) The intrusive floor is not necessarily formed by all the caps.

Finally, the minimized orientation of the caps of the capped B-CD macrocycle seems to affect the orientation of some of the secondary hydroxyls. This is not an anomaly of the scaling parameters since regardless of EEL parameter used (Table IA-IIB), the caps appear to affect the position of the secondary hydroxyls. This result is significant, in that it is possible for the caps to affect the position of the secondary hydroxyls in such a manner as to move an hydroxyl group from the rim of the cavity, in toward the cavity itself. This could potentially enhance complexation by moving one hydroxyl group into a more optimal position for nucleophilic attack on a substrate. Consequently, the rate acceleration observed by Breslow could be the combined result of capping the macrocycle and the secondary hydroxyls being in more favorable position to facilitate complexation. Additional molecular mechanics studies of the mimic-substrate complex are needed to explore this hypothesis.

C. Molecular Electrostatic Potential Maps

The electrostatic complementarity of the B-CD and capped B-CD mimics of alpha-chymotrypsin for their substrates was investigated by analysis of two dimensional molecular electrostatic potential contour maps. The

pattern of the maps was explored in order to determine how the pattern can influence the directionality of approach of a substrate to the binding site of the B-CD and capped B-CD mimics. The maps for B-CD and capped present circular symmetrical patterns, but the capped B-CD pattern appears in general to be more positive from the negative z-direction. Since the electrostatic patterns are in general quite similar, both the B-CD and capped B-CD cavities are seen to have approximately the same effect on directionality of approach of the substrate into the cavity.

D. Summary

We conclude that the rate enhancement exhibited by the capped cyclodextrins may be due to two reasons: (1) not only do the caps form an intrusive floor, pushing the substrate up into a more optimal position for interaction with the hydroxyl nucleophiles; but also (2) the caps may enhance the optimal mode of binding by moving the nucleophile toward the substrate. Further calculations are needed to investigate this hypothesis.

V. TABLES

TABLE IA

DEPENDENCE OF MINIMIZED CONFORMATIONAL ENERGY ON SCALING PARAMETERS

NB AND EEL: BETA-CYCLODEXTRIN

FILE	a T.E.	b BOND	c B.A.	d DIH.	e VDW	f ELEC	g H-B	h 1-4 VDW	i 1-4 EEL	j NB	k EEL
E	1289.0	20.40	32.90	81.12	-21.92	-409.8	-4.38	15.63	1575.0	0.5	0.5
A	1297.0	16.12	31.34	79.56	-22.91	-412.7	-4.51	15.81	1576.0	1.0	0.5
F	1274.0	14.47	30.86	81.16	-23.38	-412.3	-4.45	14.48	1579.0	1.5	0.5
G	1270.0	13.99	31.55	80.16	-23.57	-412.9	-4.49	12.66	1573.0	2.0	0.5
R	1266.0	13.17	32.47	79.37	-24.10	-414.0	-4.50	10.21	1573.0	3.0	0.5
D	474.8	8.53	12.58	71.30	-23.62	-472.3	-5.17	20.63	862.9	0.5	1.0
C	461.4	4.29	9.19	69.09	-24.52	-477.4	-5.45	17.91	868.3	1.0	1.0
B	454.3	3.10	8.12	67.82	-25.13	-480.6	-5.52	14.65	871.9	1.5	1.0
H	450.5	2.53	7.72	67.60	-25.41	-482.0	-5.60	12.42	873.2	2.0	1.0
S	446.4	2.06	7.81	67.70	-25.57	-482.9	-5.69	9.44	873.6	3.0	1.0
I	189.4	7.09	11.11	72.43	-23.20	-485.8	-5.86	21.24	592.4	0.5	1.5
J	159.1	2.86	7.53	64.96	-23.59	-509.3	-6.74	20.93	602.4	1.0	1.5
K	151.9	2.05	6.98	64.73	-24.12	-511.9	-6.90	16.24	604.8	1.5	1.5
L	147.5	1.36	6.46	66.28	-25.02	-516.4	-7.33	14.37	607.7	2.0	1.5
T	141.2	0.97	7.24	64.18	-24.95	-521.0	-7.63	11.87	610.5	3.0	1.5
M	22.9	6.72	12.22	61.98	-20.74	-512.8	-6.85	29.01	453.4	0.5	2.0
N	8.6	2.82	8.43	67.04	-23.57	-519.3	-7.45	21.77	458.9	1.0	2.0
O	-3.6	1.72	9.49	62.41	-23.37	-529.2	-8.02	20.21	463.2	1.5	2.0
P	-7.5	1.26	8.73	63.93	-24.29	-530.6	-8.27	17.40	464.4	2.0	2.0
U	-15.5	1.24	1.79	62.65	-23.22	-541.6	-8.72	13.34	469.0	3.0	2.0
X	-129.1	6.49	12.71	62.38	-20.99	-520.7	-7.31	32.13	306.2	0.5	3.0
Y	-148.9	2.78	12.10	62.85	-22.58	-525.8	-8.26	28.07	312.0	1.0	3.0
Q	-159.3	2.01	13.10	63.43	-23.20	-544.5	-8.97	23.82	315.1	1.5	3.0
Z	-165.1	1.79	14.18	63.88	-23.52	-549.4	-9.23	20.43	316.7	2.0	3.0
V	-172.2	1.70	15.51	64.44	-23.87	-554.9	-9.46	15.78	318.6	3.0	3.0

a. T.E. - TOTAL ENERGY: UNIT (Kcal/mol)

b. BOND - BOND STRETCHING

c. B.A. - BOND ANGLE BENDING

d. DIH. - TORSIONAL

e. VDW - VAN DER WAALS

f. ELEC - ELECTROSTATIC

g. H-B - HYDROGEN BONDING

h. 1-4VDW - 1-4 VAN DER WAALS

i. 1-4EEL - 1-4 ELECTROSTATIC

j. 1-4 NON-BONDED SCALING PARAMETER

k. 1-4 ELECTROSTATIC SCALING PARAMETER

TABLE IB

DEPENDENCE OF MINIMIZED CONFORMATIONAL ENERGY ON SCALING PARAMETERS

NB AND EEL: BETA-CYCLODEXTRIN

FILE	a T.E.	b BOND	c B.A.	d DIH.	e VDW	f ELEC	g H-B	h 1-4 VDW	i 1-4 EEL	j NB	k EEL
E	1289.0	20.40	32.90	81.12	-21.92	-409.8	-4.38	15.63	1575.0	0.5	0.5
D	474.8	8.53	12.58	71.30	-23.62	-472.3	-5.17	20.63	862.9	0.5	1.0
I	189.4	7.09	11.11	72.43	-23.20	-485.8	-5.86	21.24	592.4	0.5	1.5
M	23.0	6.72	12.22	61.98	-20.74	-512.8	-6.85	29.01	453.4	0.5	2.0
X	-129.1	6.49	12.71	62.38	-20.99	-520.7	-7.31	32.13	306.2	0.5	3.0
A	1279.0	16.12	31.34	79.56	-22.91	-412.7	-4.51	15.81	1576.0	1.0	0.5
C	461.4	4.29	9.19	69.09	-24.52	-477.4	-5.45	17.91	868.3	1.0	1.0
J	159.1	2.87	7.53	64.96	-23.59	-509.3	-6.74	20.93	602.4	1.0	1.5
N	8.6	2.82	8.43	67.04	-23.57	-519.3	-7.45	21.77	458.9	1.0	2.0
Y	-148.9	2.78	12.10	62.85	-22.58	-535.8	-8.26	28.07	312.0	1.0	3.0
F	1274.0	14.47	30.86	81.16	-23.38	-412.3	-4.45	14.48	1574.0	1.5	0.5
B	454.3	3.10	8.12	67.82	-25.13	-480.6	-5.52	14.65	871.9	1.5	1.0
K	151.9	2.05	6.98	64.73	-24.12	-511.9	-6.90	16.24	604.8	1.5	1.5
O	-3.6	1.72	9.49	62.41	-23.37	-529.2	-8.02	20.21	463.2	1.5	2.0
Q	-159.3	2.01	13.14	63.43	-23.20	-544.5	-8.97	23.82	315.1	1.5	3.0
G	1270.0	13.99	31.55	80.16	-23.57	-412.9	-4.49	12.66	1573.0	2.0	0.5
H	450.5	2.53	7.72	67.60	-25.41	-482.0	-5.60	12.42	873.2	2.0	1.0
L	147.5	1.36	6.46	66.28	-25.02	-516.4	-7.33	14.37	607.7	2.0	1.5
P	-7.5	1.26	8.73	63.93	-24.29	-530.6	-8.27	17.40	464.4	2.0	2.0
Z	-165.1	1.79	14.18	63.88	-23.52	-549.4	-9.23	20.43	316.7	2.0	3.0
R	1266.0	13.17	32.47	79.37	-24.10	-414.0	-4.50	10.21	1573.0	3.0	0.5
S	446.4	2.06	7.81	67.70	-25.57	-482.9	-5.69	9.44	873.6	3.0	1.0
T	141.2	0.97	7.24	64.18	-24.95	-521.0	-7.63	11.87	610.5	3.0	1.5
U	-15.5	1.24	11.79	62.65	-23.22	-541.6	-8.73	13.34	469.0	3.0	2.0
V	-172.2	1.70	15.51	64.44	-23.87	-554.9	-9.46	15.78	318.6	3.0	3.0

a. T.E. - TOTAL ENERGY: UNIT (Kcal/mol)

b. BOND - BOND STRETCHING

c. B.A. - BOND ANGLE BENDING

d. DIH. - TORSIONAL

e. VDW - VAN DER WAALS

f. ELEC - ELECTROSTATIC

g. H-B - HYDROGEN BONDING

h. 1-4VDW - 1-4 VAN DER WAALS

i. 1-4EEL - 1-4 ELECTROSTATIC

j. 1-4 NON-BONDED SCALING PARAMETER

k. 1-4 ELECTROSTATIC SCALING PARAMETER

TABLE IIA

DEPENDENCE OF MINIMIZED CONFORMATIONAL ENERGY ON SCALING PARAMETERS

NB AND EEL: CAPPED BETA-CYCLODEXTRIN

FILE	a T.E.	b BOND	c B.A.	d DIH.	e VDW	f ELEC	g H-B	h 1-4VDW	i 1-4EEL	j NB	k EEL
E	1065.0	22.47	38.54	80.84	-41.29	-467.0	-3.96	33.60	1402.0	0.5	0.5
A	1036.0	16.99	34.61	79.03	-42.86	-465.6	-4.04	32.02	1386.0	1.0	0.5
F	1043.0	15.21	35.07	84.35	-39.06	-471.9	-4.28	24.28	1399.0	1.5	0.5
G	1030.0	13.84	34.99	79.00	-42.26	-473.9	-4.10	23.65	1398.0	2.0	0.5
R	1012.00	13.16	37.17	74.14	-46.74	-471.3	-3.54	20.71	1389.0	3.0	0.5
D	329.10	9.89	18.46	64.81	-40.29	-522.0	-3.68	32.56	769.3	0.5	1.0
C	306.40	4.60	12.80	60.09	-39.34	-530.3	-4.04	28.37	774.2	1.0	1.0
B	290.90	3.63	12.37	60.01	-43.78	-531.1	-4.04	24.25	769.6	1.5	1.0
H	285.30	2.74	11.02	60.87	-45.37	-527.7	-4.26	21.17	766.9	2.0	1.0
S	279.90	2.26	10.52	61.53	-46.06	-527.2	-4.39	16.42	766.8	3.0	1.0
I	65.97	7.44	16.40	63.51	-40.38	-538.0	-4.14	36.23	524.9	0.5	1.5
J	45.30	3.03	10.99	62.96	-40.93	-543.9	-4.72	29.77	528.1	1.0	1.5
K	40.03	1.94	8.56	65.58	-42.22	-539.9	-4.82	24.34	526.6	1.5	1.5
L	34.32	1.38	8.46	66.57	-42.56	-544.3	-5.40	22.62	527.6	2.0	1.5
T	18.50	1.06	10.36	58.14	-44.52	-547.9	-4.55	16.62	529.2	3.0	1.5
M	-62.98	7.04	16.71	64.05	-40.26	-541.2	-4.27	36.62	398.3	0.5	2.0
N	-87.17	2.70	11.30	63.30	-40.82	-550.4	-4.96	30.88	400.8	1.0	2.0
O	-93.57	1.76	9.01	63.24	-41.14	-548.9	-5.05	25.30	402.2	1.5	2.0
P	-98.77	1.20	8.58	65.11	-42.11	-551.0	-5.53	22.16	402.8	2.0	2.0
U	-112.60	0.89	9.91	60.35	-43.11	-554.2	-5.31	16.95	402.0	3.0	2.0
X	-196.00	6.49	17.01	64.30	-40.64	-544.7	-4.55	38.34	267.8	0.5	3.0
Y	-220.20	2.63	12.68	64.34	-41.09	-555.1	-5.27	31.62	270.0	1.0	3.0
Q	-230.20	1.76	10.88	64.94	-41.83	-558.2	-5.51	26.06	271.7	1.5	3.0
Z	-236.10	1.65	11.00	62.69	-40.28	-558.3	-5.61	20.79	272.0	2.0	3.0
V	-241.90	1.52	9.77	63.33	-41.32	-559.3	-5.81	17.11	272.8	3.0	3.0

a. T.E. - TOTAL ENERGY: UNIT (Kcal/mol)

b. BOND - BOND STRETCHING

c. B.A. - BOND ANGLE BENDING

d. DIH. - TORSIONAL

e. VDW - VAN DER WAALS

f. ELEC - ELECTROSTATIC

g. H-B - HYDROGEN BONDING

h. 1-4VDW - 1-4 VAN DER WAALS

i. 1-4EEL - 1-4 ELECTROSTATIC

j. 1-4 NON-BONDED SCALING PARAMETER

k. 1-4 ELECTROSTATIC SCALING PARAMETER

TABLE IIB

DEPENDENCE OF MINIMIZED CONFORMATIONAL ENERGY ON SCALING PARAMETERS NB AND EEL: CAPPED BETA-CYCLODEXTRIN

FILE	a T.E.	b BOND	c B.A.	d DIH.	e VDW	f ELEC	g H-B	h 1-4VDW	i 1-4EEL	j NB	k EEL
E	1065.00	22.47	38.54	80.84	-41.29	-467.0	-3.96	33.60	1402.0	0.5	0.5
D	329.10	9.89	18.46	64.81	-40.29	-522.0	-3.68	32.56	769.3	0.5	1.0
I	65.97	7.44	16.40	63.51	-40.38	-538.0	-4.14	36.23	524.9	0.5	1.5
M	-62.98	7.04	16.71	64.05	-40.26	-541.2	-4.27	36.62	398.3	0.5	2.0
X	-196.00	6.49	17.01	64.30	-40.64	-544.7	-4.55	38.34	267.8	0.5	3.0
A	1036.00	16.99	34.61	79.03	-42.86	-465.6	-4.04	32.02	1386.0	1.0	0.5
C	306.40	4.60	12.80	60.09	-39.34	-530.3	-4.04	28.37	774.2	1.0	1.0
J	45.30	3.03	10.99	62.96	-40.93	-543.9	-4.72	29.77	528.1	1.0	1.5
N	-87.17	2.70	11.30	63.30	-40.82	-550.4	-4.96	30.88	400.8	1.0	2.0
Y	-220.20	2.63	12.68	64.34	-41.09	-555.1	-5.27	31.62	270.0	1.0	3.0
F	1043.00	15.21	35.07	84.35	-39.06	-471.9	-4.28	24.28	1399.0	1.5	0.5
B	290.90	3.63	12.37	60.01	-43.78	-531.1	-4.04	24.25	769.6	1.5	1.0
K	40.03	1.94	8.56	65.58	-42.22	-539.9	-4.82	24.34	526.6	1.5	1.5
O	-93.57	1.76	9.01	63.24	-41.14	-548.9	-5.05	25.30	402.2	1.5	2.0
Q	-230.20	1.76	10.88	64.94	-41.83	-558.2	-5.51	26.06	271.7	1.5	3.0
G	1030.00	13.84	34.99	79.00	-42.26	-473.9	-4.10	23.65	1398.0	2.0	0.5
H	285.30	2.74	11.02	60.87	-45.37	-527.7	-4.26	21.17	766.9	2.0	1.0
L	34.32	1.38	8.46	66.57	-42.56	-544.3	-5.40	22.62	527.6	2.0	1.5
P	-98.77	1.20	8.58	65.11	-42.11	-551.0	-5.53	22.16	402.8	2.0	2.0
Z	-236.10	1.65	11.00	62.69	-40.28	-558.3	-5.61	20.79	272.0	2.0	3.0
R	1012.00	13.16	37.17	74.14	-46.74	-471.3	-3.54	20.71	1389.0	3.0	0.5
S	279.90	2.26	10.52	61.53	-46.06	-527.2	-4.39	16.42	766.8	3.0	1.0
T	18.50	1.06	10.36	58.14	-44.52	-547.9	-4.55	16.62	529.2	3.0	1.5
U	-112.60	0.89	9.91	60.35	-43.11	-554.2	-5.31	16.95	402.0	3.0	2.0
V	-241.90	1.52	9.77	63.33	-41.32	-559.3	-5.81	17.11	272.8	3.0	3.0

a. T.E. - TOTAL ENERGY: UNIT (Kcal/mol)
b. BOND - BOND STRETCHING
c. B.A. - BOND ANGLE BENDING
d. DIH. - TORSIONAL
e. VDW - VAN DER WAALS
f. ELEC - ELECTROSTATIC
g. H-B - HYDROGEN BONDING
h. 1-4VDW - 1-4 VAN DER WAALS
i. 1-4EEL - 1-4 ELECTROSTATIC
j. 1-4 NON-BONDED SCALING PARAMETER
k. 1-4 ELECTROSTATIC SCALING PARAMETER

TABLE IIIA

INTRAMOLECULAR HYDROGEN BONDING INTERACTIONS: BETA-CYCLODEXTRIN [a]

Atom 1	Fragment IN Number	Atom 2	Fragment IN Number	Hydrogen-Bond Distances (A) [b]
H4	1	O6	7	1.77
H4	2	O6	3	1.87
H4	3	O6	4	1.89
H4	4	O6	5	1.99
H4	5	O6	6	1.99
H4	6	O6	7	1.87

a. From File C, Table IA, NB = 1.0, EEL = 1.0.

b. Hydrogen-bond distances are between Atom 1 and Atom 2 in different fragments.

TABLE IIIB

INTRAMOLECULAR HYDROGEN BONDING INTERACTIONS: CAPPED BETA-CYCLODEXTRIN [a]

Atom 1	Fragment IN Number	Atom 2	Fragment IN Number	Hydrogen-Bond Distances (A)[b]
H4	1	O6	7	1.77
H4	2	O6	3	1.87
H4	3	O6	4	1.89
H4	4	O6	5	1.99
H4	5	O6	6	1.99
H4	6	O6	7	1.87

a. From File C, Table IIA, NB = 1.0, EEL = 1.0.

b. Hydrogen-bond distances are between Atom 1 and Atom 2 in different fragments.

TABLE IVA

STATISTICAL ANALYSIS OF FIT OF CALCULATED CONFORMATION

TO X-RAY STRUCTURE: BETA CYCLODEXTRIN

F	a T.E.	b RMS DEVIATIONS 77 ATOMS	ALL ATOMS	c MEAN	d STD. DEV.	e MAX. DEV.	f FOR ATOM	g NB	h EEL
E	1289.0	0.4775	0.4232	0.293	0.305	2.580	H68	0.5	0.5
A	1279.0	0.5347	0.4740	0.322	0.347	2.440	H68	1.0	0.5
F	1274.0	0.5668	0.5024	0.339	0.371	2.459	H54	1.5	0.5
G	1270.0	0.5954	0.5278	0.358	0.388	2.539	H54	2.0	0.5
D	474.8	0.2335	0.2070	0.151	0.142	1.235	H68	0.5	1.0
C	461.4	0.2291	0.2030	0.141	0.146	1.136	H68	1.0	1.0
B	454.3	0.2598	0.2303	0.165	0.161	1.032	H82	1.5	1.0
H	450.5	0.2674	0.2370	0.169	0.166	1.018	H68	2.0	1.0
I	189.4	0.2637	0.2337	0.161	0.170	0.990	039	0.5	1.5
J	159.1	0.4238	0.3757	0.254	0.277	1.542	H40	1.0	1.5
K	151.9	0.4465	0.3598	0.272	0.287	1.745	H68	1.5	1.5
L	147.5	0.3666	0.3250	0.226	0.234	1.678	H68	2.0	1.5
M	23.0	0.7152	0.6339	0.437	0.459	2.692	H40	0.5	2.0
N	8.6	0.3811	0.3378	0.233	0.225	1.745	H68	1.0	2.0
O	3.6	0.5904	0.5234	0.352	0.387	2.124	H40	1.5	2.0
P	7.5	0.5211	0.4619	0.320	0.334	1.937	H68	2.0	2.0
X	129.1	0.7324	0.6492	0.448	0.470	2.739	H40	0.5	3.0
Y	148.9	0.6797	0.5980	0.405	0.440	2.335	H40	1.0	3.0
Z	165.1	0.7012	0.6216	0.426	0.453	2.397	H40	2.0	3.0
Q	159.3	0.7018	0.6221	0.424	0.455	2.422	H40	1.5	3.0

a. TOTAL MINIMIZED ENERGY.

b. FOR 77 ATOMS IN FIT AND FOR ALL 98 ATOMS IN MOLECULE.

c. MEAN CALCULATED FOR ALL 98 ATOMS.

d. STD DEV - STANDARD DEVIATION FOR ALL 98 ATOMS.

e. THE MAXIMUM DEVIATION FROM THE MEAN IS FOR THE ATOM GIVEN IN THE NEXT COLUMN (f).

g. 1-4 NON-BONDING SCALING PARAMETER.

h. 1-4 ELECTROSTATIC SCALING PARAMETER.

TABLE IVB

STATISTICAL ANALYSIS OF FIT OF CALCULATED CONFORMATION

TO X-RAY STRUCTURE: BETA CYCLODEXTRIN

F	a T.E.	b RMS DEVIATIONS 77 ATOMS	ALL ATOMS	c MEAN	d STD. DEV.	e MAX. DEV.	f FOR ATOM	g NB	h EEL
E	1289.0	0.4775	0.4232	0.293	0.305	2.580	H68	0.5	0.5
D	474.8	0.2335	0.2070	0.151	0.142	1.235	H68	0.5	1.0
I	189.4	0.2637	0.2337	0.161	0.170	0.990	039	0.5	1.5
M	23.0	0.7152	0.6339	0.437	0.459	2.692	H40	0.5	2.0
X	-129.1	0.7324	0.6492	0.448	0.470	2.739	H40	0.5	3.0
A	1279.0	0.5347	0.4740	0.322	0.347	2.440	H68	1.0	0.5
C	461.4	0.2291	0.2030	0.141	0.145	1.136	H68	1.0	1.0
J	159.1	0.4238	0.3757	0.254	0.277	1.542	H40	1.0	1.5
N	8.6	0.3811	0.3378	0.233	0.245	1.745	H68	1.0	2.0
Y	-148.9	0.6797	0.5980	0.405	0.440	2.335	H40	1.0	3.0
F	1274.0	0.5668	0.5024	0.339	0.371	2.459	H54	1.5	0.5
B	454.3	0.2598	0.2303	0.165	0.161	1.032	H82	1.5	1.0
K	151.9	0.4465	0.3598	0.272	0.287	1.745	H68	1.5	1.5
O	-3.6	0.5904	0.5234	0.352	0.387	2.124	H40	1.5	2.0
Q	-159.3	0.7018	0.6221	0.424	0.455	2.422	H40	1.5	3.0
G	1270.0	0.5954	0.5278	0.358	0.388	2.539	H54	2.0	0.5
H	450.5	0.2674	0.2370	0.169	0.166	1.018	H68	2.0	1.0
L	147.5	0.3666	0.3250	0.226	0.234	1.678	H68	2.0	1.5
P	-7.5	0.5211	0.4619	0.320	0.334	1.937	H68	2.0	2.0
Z	-165.1	0.7012	0.6216	0.426	0.453	2.397	H40	2.0	3.0

a. TOTAL MINIMIZED ENERGY.

b. FOR 77 ATOMS IN FIT AND FOR ALL 98 ATOMS IN MOLECULE.

c. MEAN CALCULATED FOR ALL 98 ATOMS.

d. STD DEV - STANDARD DEVIATION FOR ALL 98 ATOMS

e. THE MAXIMUM DEVIATION FROM THE MEAN IS FOR THE ATOM GIVEN IN THE NEXT COLUMN (f).

g. 1-4 NON-BONDING SCALING PARAMETER.

h. 1-4 ELECTROSTATIC SCALING PARAMETER.

TABLE VA

STATISTICAL ANALYSIS OF FIT OF CALCULATED CONFORMATION

TO X-RAY STRUCTURE: CAPPED BETA CYCLODEXTRIN

	a	b		c	d	e	f	g	h
F	T.E.	RMS DEVIATIONS 70 ATOMS	ALL ATOMS	MEAN	STD. DEV.	MAX. DEV.	FOR ATOM	NB	EEL
E	1065.0	0.5294	0.4185	0.293	0.299	4.477	O14	0.5	0.5
A	1036.0	0.6073	0.4801	0.328	0.351	4.078	O62	1.0	0.5
F	1043.0	0.5915	0.4676	0.323	0.338	4.109	O62	1.5	0.5
G	1030.0	0.6704	0.5300	0.367	0.383	4.031	O62	2.0	0.5
D	329.1	0.6961	0.5503	0.375	0.403	5.235	O62	0.5	1.0
C	306.40	0.8146	0.6440	0.418	0.490	5.596	O62	1.0	1.0
B	290.90	0.7246	0.5729	0.373	0.435	5.232	O62	1.5	1.0
H	285.30	0.7618	0.6022	0.389	0.460	5.200	O62	2.0	1.0
I	65.97	0.8372	0.6618	0.443	0.492	5.869	O62	0.5	1.5
J	45.30	0.7687	0.6077	0.389	0.467	5.463	O62	1.0	1.5
K	40.03	0.5614	0.4439	0.284	0.341	4.646	O62	1.5	1.5
L	34.32	0.5029	0.3976	0.265	0.297	4.436	O62	2.0	1.5
M	-62.98	0.7582	0.5994	0.415	0.433	5.276	O62	0.5	2.0
N	-87.17	0.7556	0.5974	0.389	0.453	5.386	O62	1.0	2.0
O	-93.57	0.6359	0.5027	0.328	0.381	4.768	O62	1.5	2.0
P	-98.77	0.5207	0.4116	0.291	0.291	4.441	O11	2.0	2.0
X	-196.00	0.6927	0.5476	0.376	0.399	4.994	O62	0.5	3.0
Y	-220.20	0.8170	0.6459	0.427	0.485	5.318	O62	1.0	3.0
Q	-230.20	0.7599	0.6007	0.405	0.444	4.801	O110	1.5	3.0
Z	-236.10	0.7348	0.5809	0.393	0.428	4.689	O110	2.0	3.0

a. TOTAL MINIMIZED ENERGY.

b. FOR 70 ATOMS IN FIT AND FOR ALL 112 ATOMS IN MOLECULE.

c. MEAN CALCULATED FOR ALL 112 ATOMS.

d. STD DEV - STANDARD DEVIATION FOR ALL 112 ATOMS.

e. THE MAXIMUM DEVIATION FROM THE MEAN IS FOR THE ATOM GIVEN IN THE NEXT COLUMN (f).

g. 1-4 NON-BONDING SCALING PARAMETER.

h. 1-4 ELECTROSTRATIC SCALING PARAMETER.

TABLE VB

STATISTICAL ANALYSIS OF FIT OF CALCULATED CONFORMATION

TO X-RAY STRUCTURE: CAPPED BETA CYCLODEXTRIN

	a	b		c	d	e	f	g	h
F	T.E.	RMS DEVIATIONS 70 ATOMS	ALL ATOMS	MEAN	STD. DEV.	MAX. DEV.	FOR ATOM	NB	EEL
E	1065.00	0.5294	0.4185	0.293	0.299	4.477	O14	0.5	0.5
D	329.10	0.6961	0.5503	0.375	0.403	5.235	O62	0.5	1.0
I	65.97	0.8372	0.6618	0.443	0.492	5.869	O62	0.5	1.5
M	-62.98	0.7582	0.5994	0.415	0.433	5.276	O62	0.5	2.0
X	-196.00	0.6927	0.5476	0.376	0.399	4.994	O62	0.5	3.0
A	1036.00	0.6073	0.4801	0.328	0.351	4.078	O62	1.0	0.5
C	306.40	0.8146	0.6440	0.418	0.490	5.596	O62	1.0	1.0
J	45.30	0.7687	0.6077	0.389	0.467	5.463	O62	1.0	1.5
N	-87.17	0.7556	0.5974	0.389	0.453	5.388	O62	1.0	2.0
Y	-220.20	0.8170	0.6459	0.427	0.485	5.318	O62	1.0	3.0
F	1043.00	0.5915	0.4676	0.323	0.338	4.109	O62	1.5	0.5
B	290.90	0.7246	0.5729	0.373	0.435	5.232	O62	1.5	1.0
K	40.03	0.5614	0.4439	0.284	0.341	4.646	O62	1.5	1.5
O	-93.57	0.6359	0.5027	0.328	0.381	4.768	O62	1.5	2.0
Q	-230.20	0.7599	0.6007	0.405	0.444	4.801	O110	1.5	3.0
G	1030.00	0.6704	0.5300	0.367	0.383	4.031	O62	2.0	0.5
H	285.30	0.7618	0.6022	0.389	0.460	5.200	O62	2.0	1.0
L	34.32	0.5029	0.3976	0.265	0.297	4.436	O62	2.0	1.5
P	-98.77	0.5207	0.4116	0.291	0.291	4.441	O110	2.0	2.0
Z	-236.10	0.7348	0.5809	0.393	0.428	4.689	O110	2.0	3.0

a. TOTAL MINIMIZED ENERGY.

b. FOR 70 ATOMS IN FIT AND FOR ALL 112 ATOMS IN MOLECULE.

c. MEAN CALCULATED FOR ALL 112 ATOMS.

d. STD DEV - STANDARD DEVIATION FOR ALL 112 ATOMS.

e. MAXIMUM DEVIATION FROM THE MEAN IS FOR THE ATOM GIVEN IN THE NEXT COLUMN (f).

g. 1-4 NON-BONDING SCALING PARAMETER.

h. 1-4 ELECTROSTATIC SCALING PARAMETER.

TABLE VIA

COMPARISON of CALCULATED and X-ray OXYGEN (O3) POSITIONS: BETA CYCLODEXTRIN [a,b]

Fragment Number	EEL				
	0.5	1.0	1.5	2.0	3.0
1	0.756	0.205	0.291	0.339	0.386
2	0.615	0.127	0.285	0.246	0.331
3	0.365	0.170	0.693	0.445	1.342
4	0.377	0.195	0.191	0.139	0.450
5	0.093	0.166	0.157	0.175	0.172
6	0.205	0.360	0.632	0.205	1.077
7	0.278	0.189	0.458	0.278	0.931

a. All deviations are given in Angstroms.

b. NB = 1.0

Table VIB

COMPARISON of CALCULATED and X-ray OXYGEN (O6) POSITIONS: BETA-CYCLODEXTRIN [a,b]

Fragment Number	EEL 0.5	1.0	1.5	2.0	3.0
1	0.806	0.160	0.108	0.032	0.195
2	0.557	0.235	0.396	0.361	0.402
3	0.369	0.248	0.794	0.537	1.566
4	0.307	0.056	0.116	0.089	0.301
5	0.817	0.154	0.247	0.392	0.402
6	0.384	0.329	0.550	0.384	0.812
7	0.595	0.224	0.243	0.595	0.680

a. All deviations are given in Angstroms.

b. NB=1.0.

Table VIIA

COMPARISON of CALCULATED and X-ray OXYGEN (O3) POSITIONS: CAPPED BETA-CYCLODEXTRIN [a,b]

Fragment Number	EEL 0.5	1.0	1.5	2.0	3.0
1	1.3899	1.4311	0.3442	0.3261	0.3037
2	0.7139	0.4959	0.4911	0.4597	0.5276
3	0.3943	0.2509	0.1112	0.2093	0.3100
4	0.9336	2.3272	2.1553	2.0109	2.0657
5	0.0489	0.4121	0.2919	0.3851	0.4392
6	0.4019	1.1087	1.3161	1.2708	1.5163
7	0.5736	0.6686	1.1320	1.1743	1.1844

a. All deviations are given in Angstroms.

b. NB=1.0

Table VIIB

COMPARISON of CALCULATED and X-ray OXYGEN (O6) POSITIONS: CAPPED BETA-CYCLODEXTRIN [a,b]

Fragment Number	EEL				
	0.5	1.0	1.5	2.0	3.0
1	1.4352	1.5145	0.2337	0.1917	0.2534
2	0.6180	0.6265	0.4275	0.4168	0.4933
3	0.6315	0.1965	0.1673	0.2869	0.3241
4	0.7923	2.2394	2.0241	1.9822	1.9692
5	0.4348	0.5148	0.6186	0.6369	0.6972
6	0.3907	0.7716	0.7775	0.7534	0.9540
7	0.6576	0.6311	0.7352	0.7806	0.7976

a. All deviations are given in Angstroms.

b. NB=1.0

TABLE VIII

ATOMIC POINT CHARGES FOR FRAGMENTS

ATOM	CHARGE	
	GLUCOSE	CAPPED GLUCOSE
C1	0.1779	0.1481
C2	0.2687	0.2375
O3	-0.5452	-0.5316
H4	0.2670	0.2706
C5	0.4826	0.5029
O6	-0.5852	-0.5605
H7	0.2970	0.2830
O8	-0.5027	-0.4474
C9	0.3887	0.4459
C10	0.1661	0.1226
O11 [a]	-0.4991	
H12 [a]	0.3200	
C13 (C15) [b]	-0.0696	-0.1140
O14 (O16) [b]	-0.1664	-0.1863
N11 [a]		-0.4490
C12 [a]		0.2037
C13 [a]		0.4728
O14 [a]		-0.3983

a. O11 and H12 are found only in the glucose fragment, while N11, C12, C13, and O14 are found only in the capped glucose fragment.

b. C13 of the glucose fragment is the same as C15 of the capped glucose fragment (Figures 6 and 19). O14 of the glucose fragment is equivalent to O16 of the capped glucose fragment.

VI. FIGURES

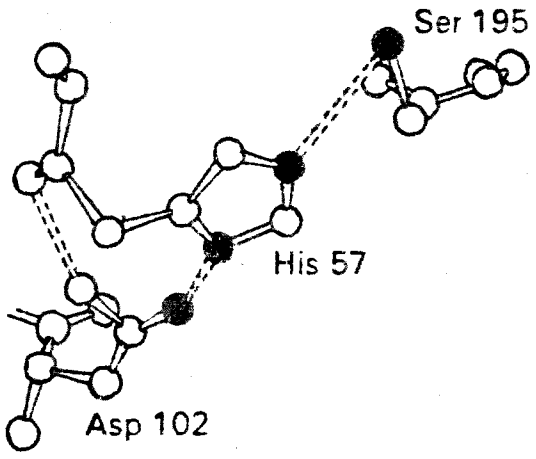

Figure 1.

Catalytic triad in chymotrypsin. His-57 is adjacent to Ser-195 which is adjacent to the carbonyl side chain of Asp-102. Reproduced from Stryer, L. Biochemistry; W.H. Freeman and Co., p. 163.

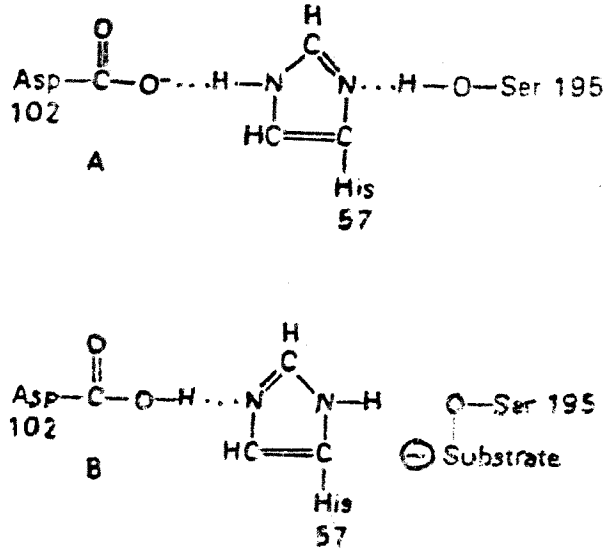

Figure 2.

Charge relay network in chymotrypsin: (A) isolated enzyme; (B) on addition of a substrate, Asp-102 and His-57 transiently bind a proton. Reproduced from Stryer, L. Biochemistry; W.H. Freeman and Co., p. 163.

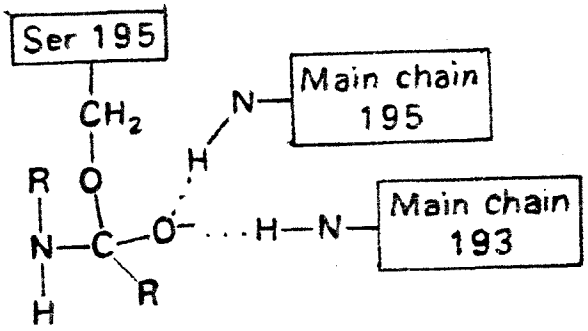

Figure 3.

The tetrahedral transition-state intermediate in the acylation and deacylation reactions of chymotrypsin. The hydrogen bonds formed by two NH groups from the main chain of the enzyme are critical in stabilizing this intermediate. Reproduced from Stryer, L. Biochemistry; W.H. Freeman and Co., p. 164.

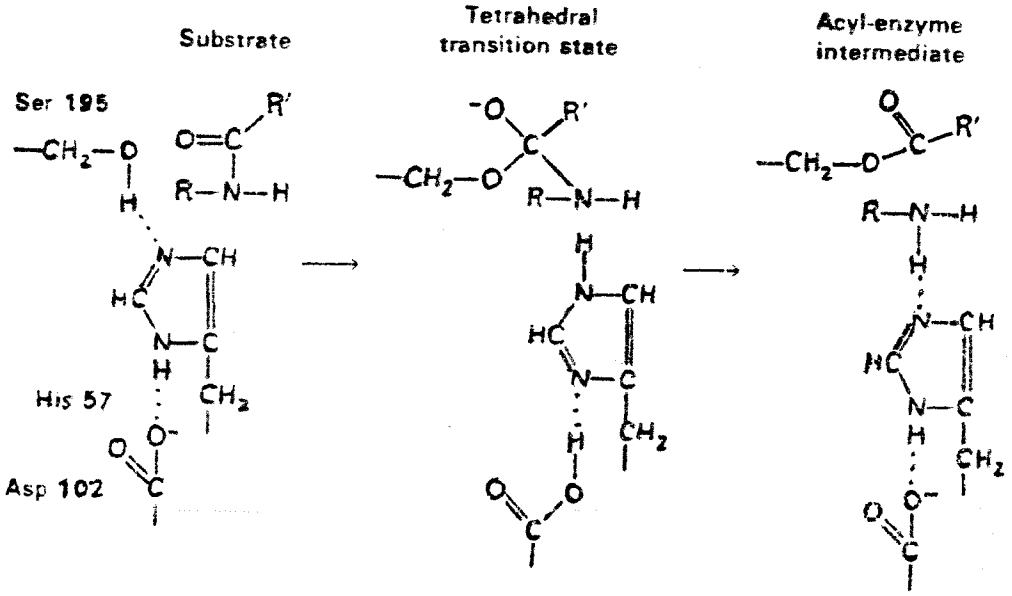

Figure 4.

First stage in the hydrolysis of a peptide bond by chymotrypsin: acylation. A tetrahedral transition state is formed. The amine component then rapidly diffuses away, which leaves an acyl-enzyme intermediate. Reproduced from Stryer, L. Biochemistry; W.H. Freeman and Co., p. 164.

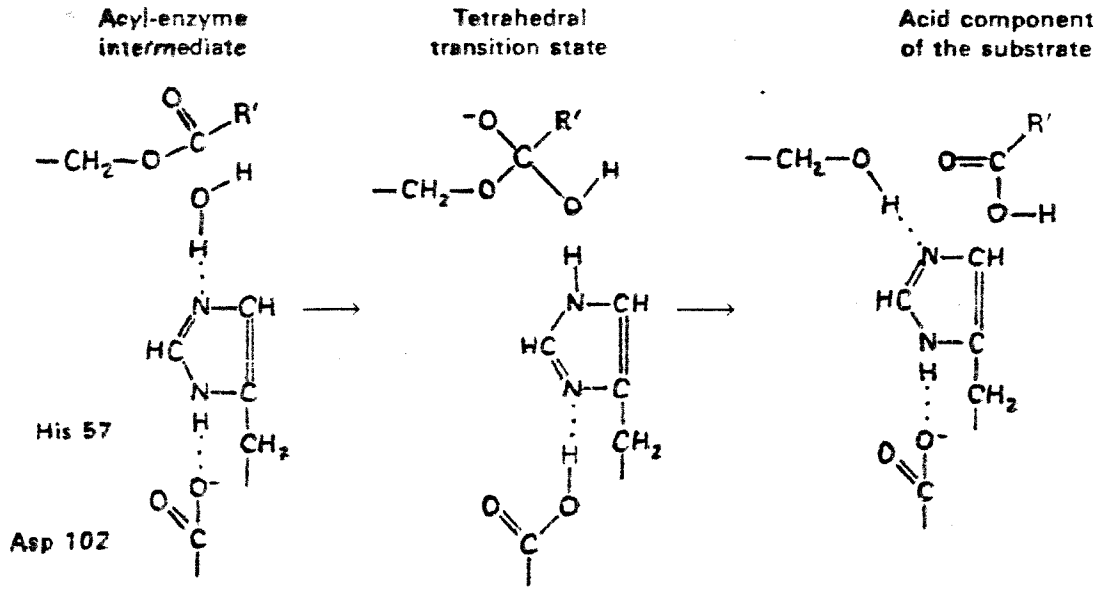

Figure 5.

Second stage in the hydrolysis of a peptide bond by chymotrypsin: deacylation. The acyl-enzyme intermediate is hydrolyzed by water. Reproduced from Stryer, L. Biochemistry; W.H. Freeman and Co., p. 165.

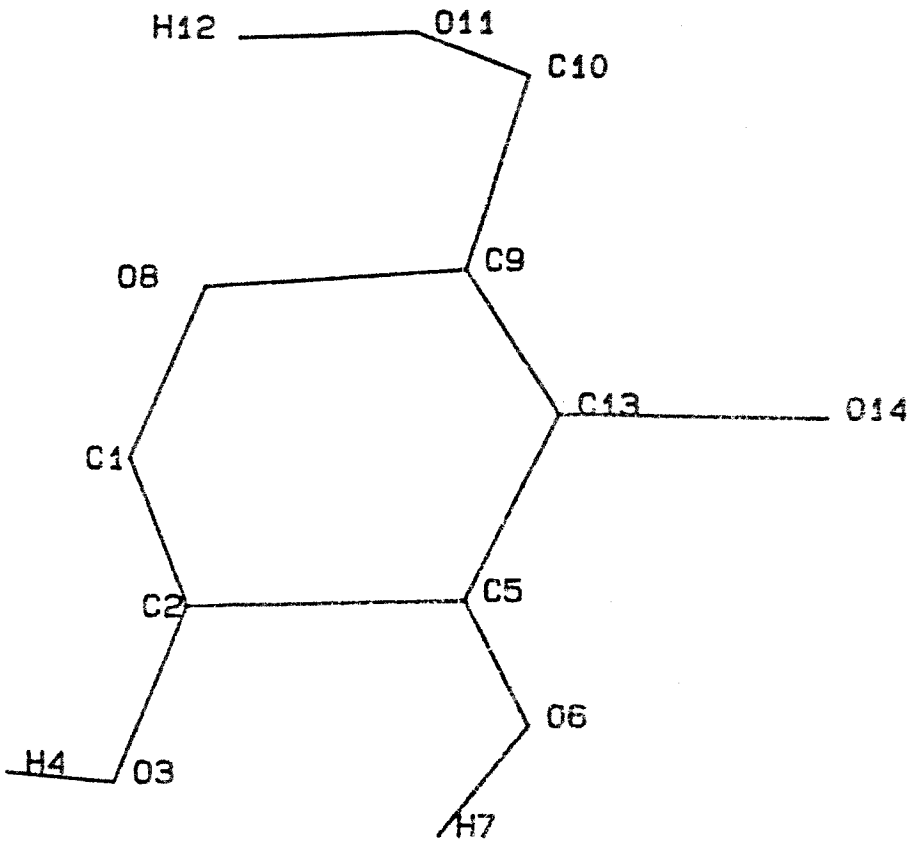

Figure 6.

The labeling scheme used in the present study to number the atoms within a glucose fragment. The primary oxygen is O11, while the secondary oxygens are O3 and O6.

Secondary oxygens (O3, O6) on the "Top"

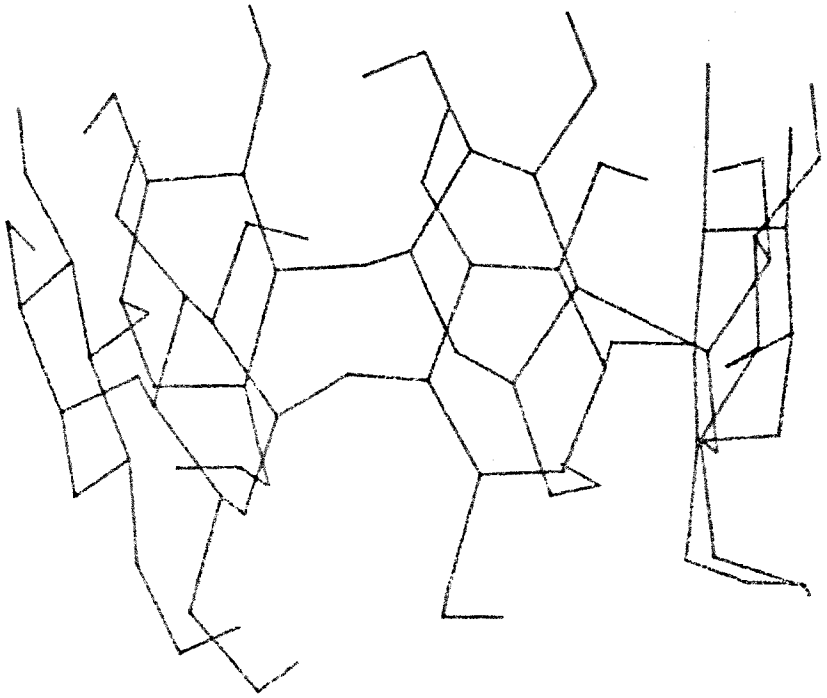

Primary oxygens (O11) on the "Bottom"

Figure 7.

Orientation of the primary and secondary hydroxyl oxygens of the B-CD X-ray crystal structure. The primary hydroxyl oxygens are in the O11 position of Figure 6; the secondary hydroxyl oxygens are in the O3 and O6 positions of Figure 6. Coordinates obtained from Harata, K. Bull. Chem. Soc. Jpn. 1982, 55, 2315-2320.

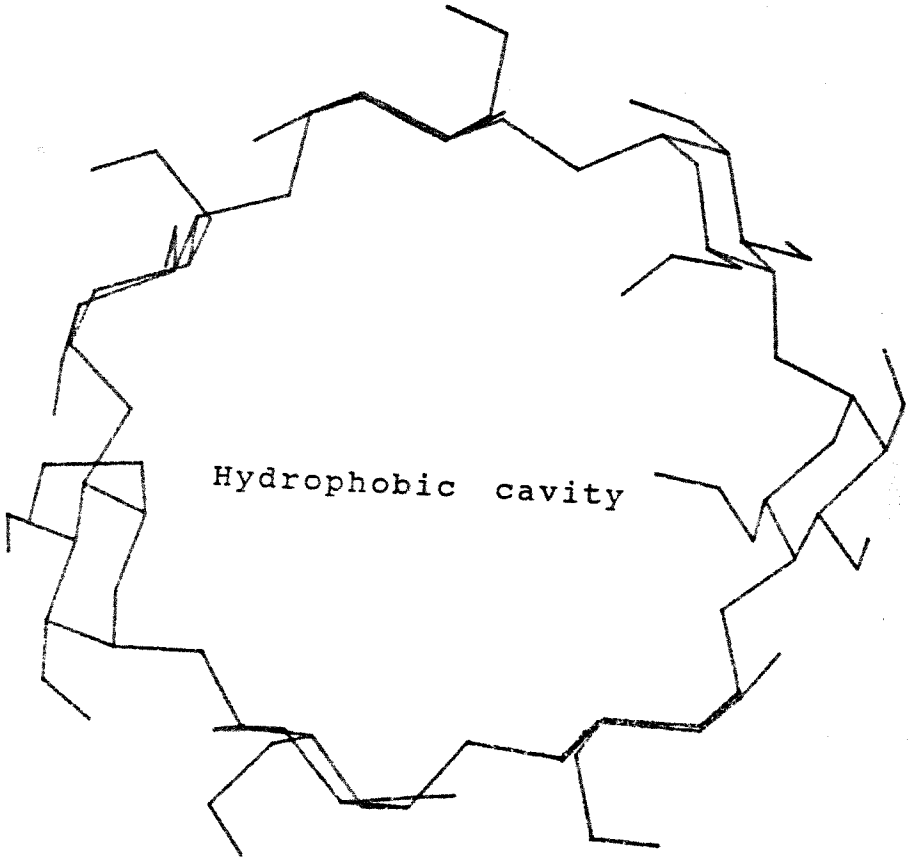

Figure 8.

Hydrophobic cavity of the X-ray B-CD macrocycle. Coordinates obtained from Harata, K. Bull. Chem. Soc. Jpn. 1982, 55, 2315-2320.

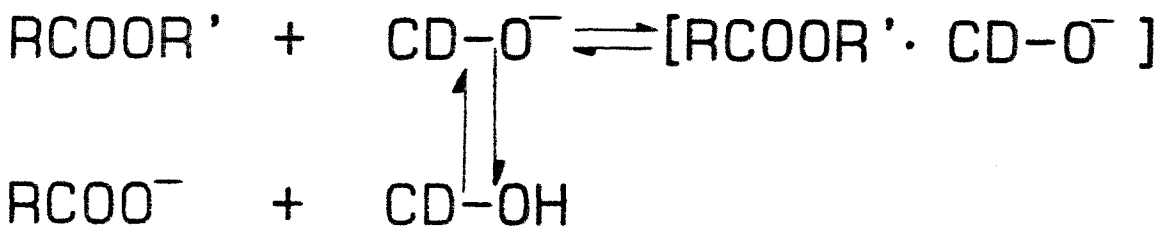

Figure 9.

Mechanism of acetylation of a cyclodextrin hydroxyl by bound phenyl acetate ester. Reproduced from Bender,M.L.; Bergeron, R.J.; Komiyama,M. The Bioorganic Chemistry of Enzyme Catalysis; John Wiley and Sons: New York, 1984, p. 511.

Figure 10.

Release of leaving group from substrate that is bound by B-CD. Reproduced from Komiyama, M.; Bender, M.L. The Chemistry of Enzyme Action; Page M.I. Ed.; Elsevier: New York, 1984, p. 511.

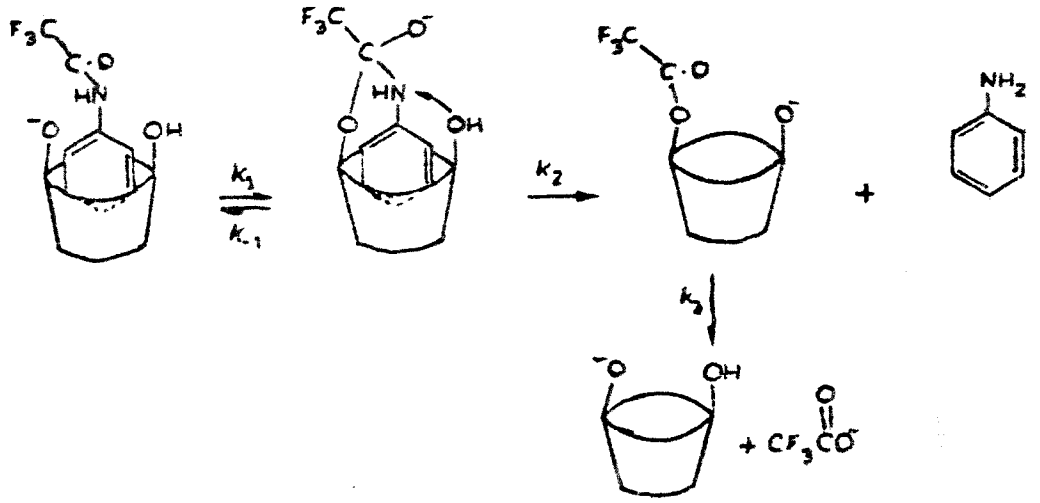

Figure 11.

General acid catalysis mechanism displayed by B-CD. Reproduced from Komiyama, M.; Bender, M.L. The Chemistry of Enzyme Action; Page M.I. Ed.; Elsevier: New York, 1984, p. 512.

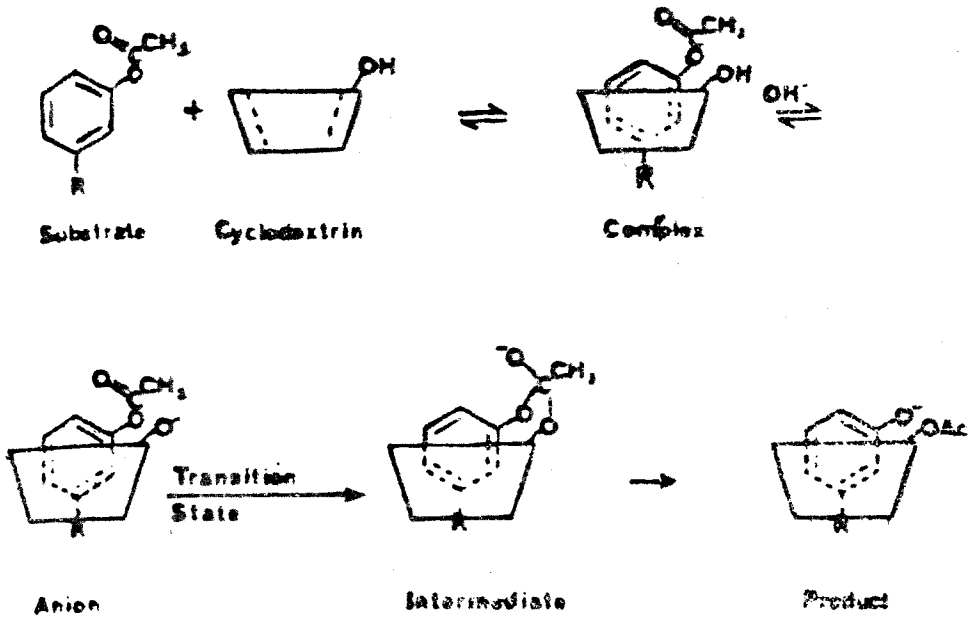

Figure 12.

Formation of B-CD tert-butylphenyl substrate transition state. Reproduced from Breslow, R.; Czarniecki, M.F.; Emert, J.; Hamaguchi, H. J. Am. Chem. Soc. 1980, 102, 762-769.

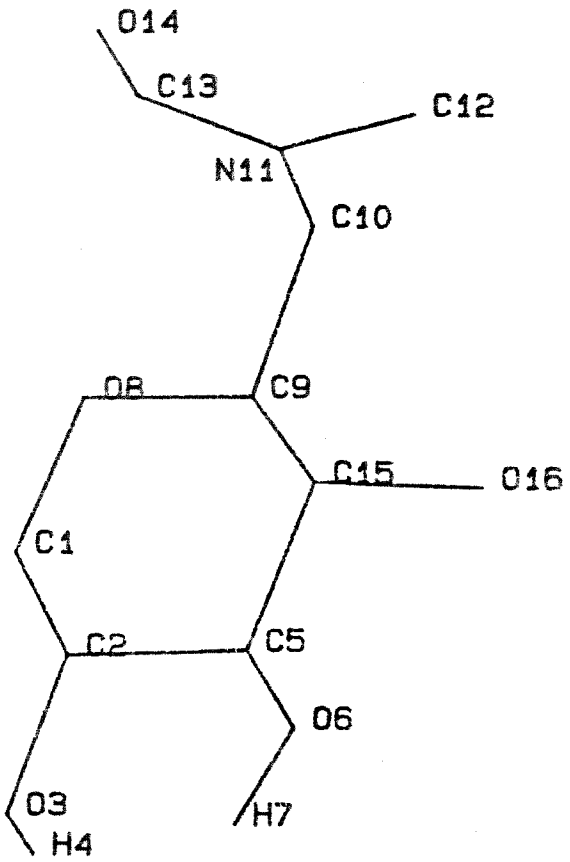

Figure 13.

Labeling scheme used in the present study to number a capped B-CD fragment. The atoms of the caps replaced the O11 hydroxyl group in the glucose fragment (Figure 6).

Secondary oxygens (O3, O6) on the "Top"

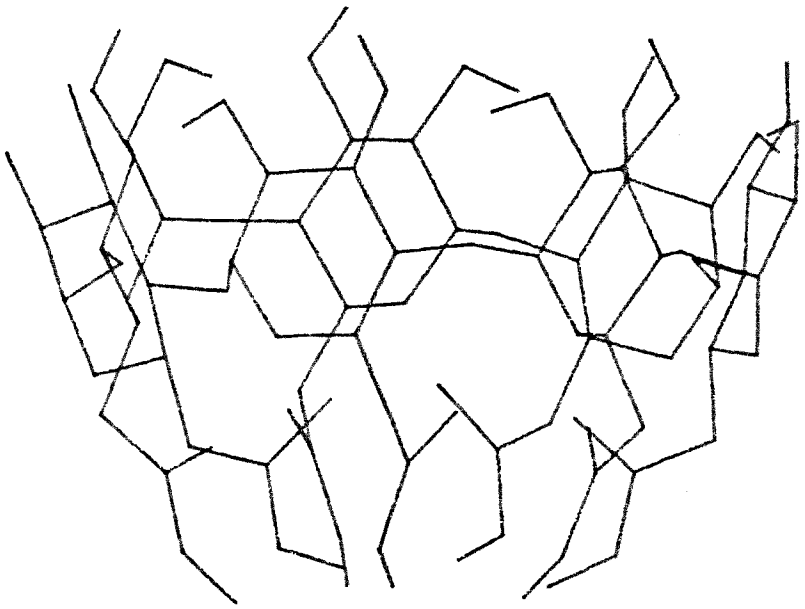

Caps forming intrusive floor on the "Bottom"

Figure 14.

Capped B-CD macrocycle produced by the EDIT module of AMBER [17]. All the caps form an intrusive floor into the cavity.

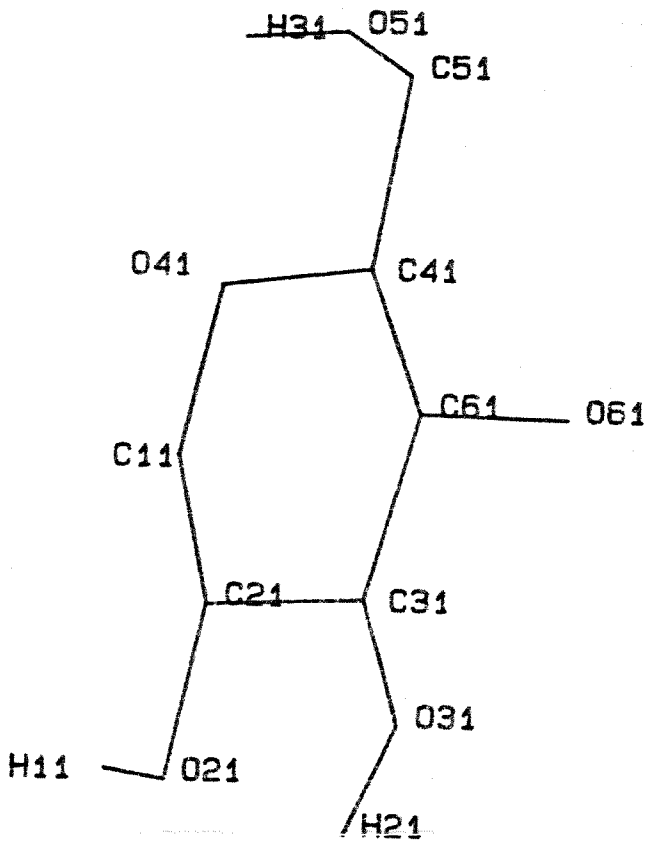

Figure 15.

Crystallographic labeling scheme for the glucose fragment. Note that, for example, C41 of Figure 15 is atom C13 of Figure 6 and C15 of Figure 13. The last number (in this case, 1) indicates the fragment to which the atom belongs; H11 is the first hydrogen atom of fragment 1, H21 is the second hydrogen atom of fragment 1. Taken from: Harata, K. Bull. Chem. Soc. Jpn. 1982, 55, 2315-2320.

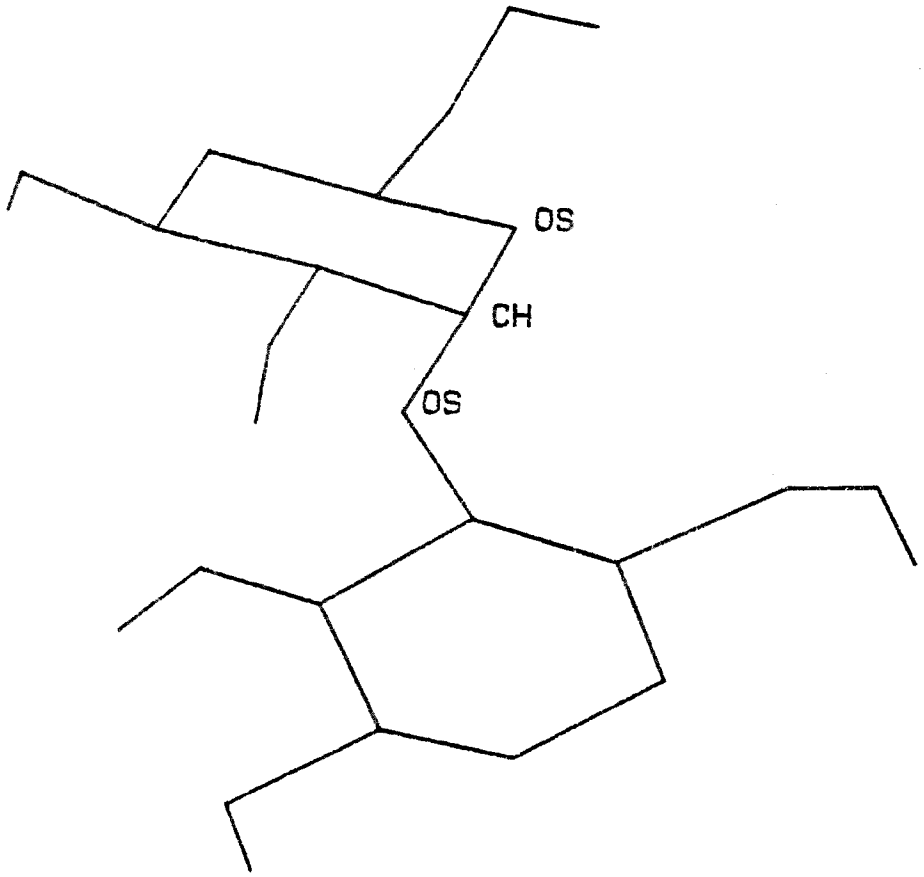

Figure 16.

The bond angle from glucose fragments that required additional angle bending parameters for the PARM module of AMBER [17]. Two glucose fragments are shown.

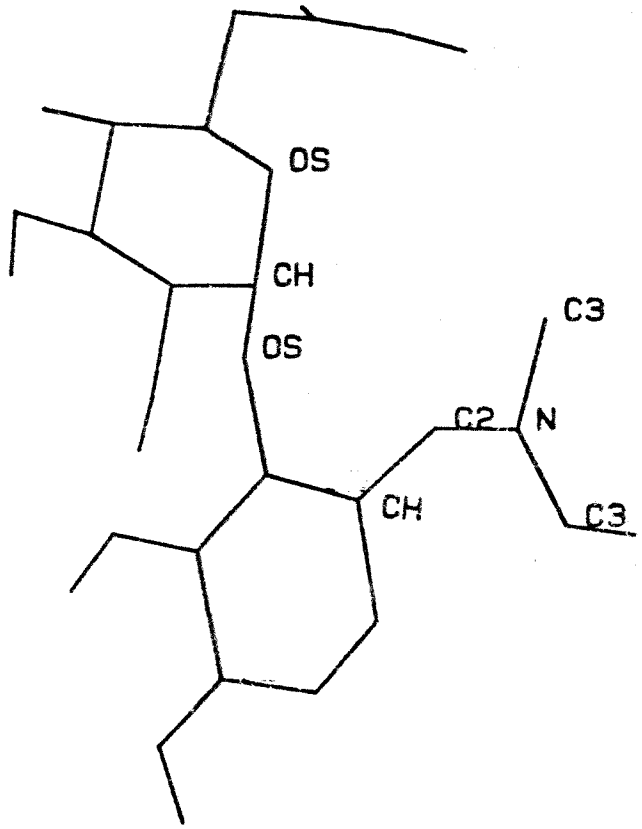

Figure 17.

The bond angles from capped glucose fragment that required additional angle bending parameters for the PARM module of AMBER [17]. Two capped glucose fragments are shown.

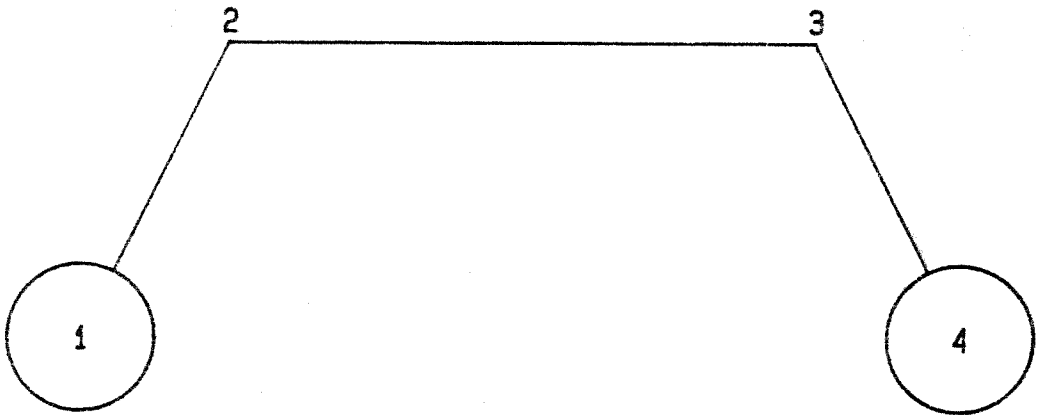

Figure 18.

Schematic of a possible 1-4 non-bonded interaction. Reproduced from Burkert, U.; Allinger, N.L. Molecular Mechanics; American Chemical Society: Washington, D.C., 1982, p. 4. Atoms 1 and 4 are drawn in a ball model, while atoms 2 and 3 are labeled. Atoms 1 and 4 are involved in the possible 1-4 nonbonded interaction.

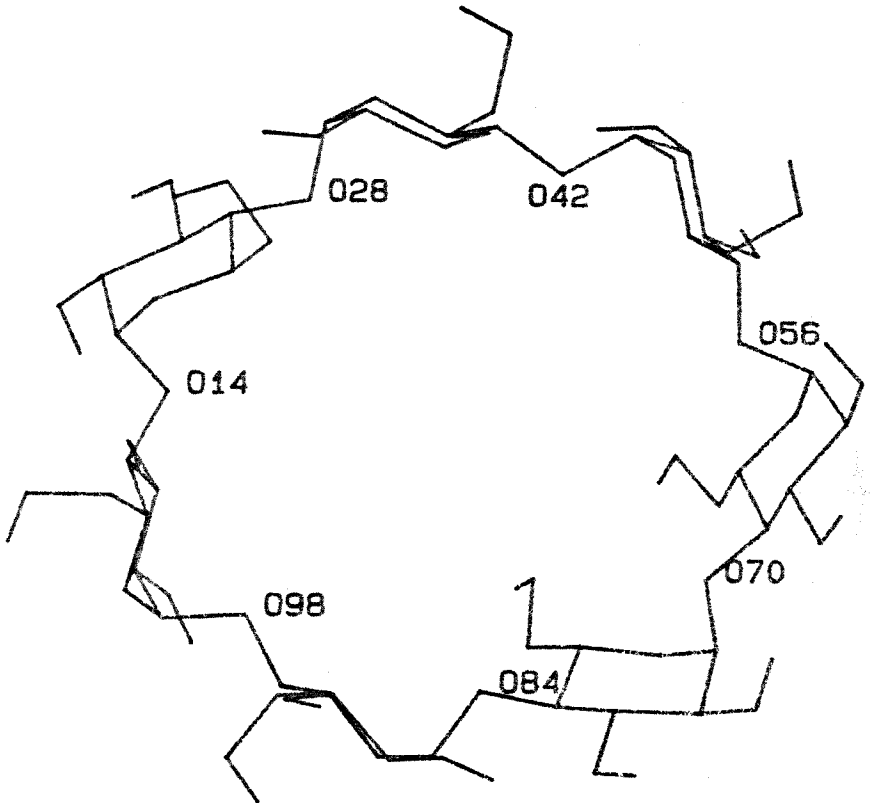

Figure 19.

The B-CD macrocycle showing the glycosidic oxygens used to define a plane for the X-ray macrocycle, prior to performing the RMS fit procedure. These atoms were also used to define the coordinates of the centroid ("dummy" atom). This "dummy" atom was then translated "up" and "down" the z-axis.

Secondary oxygens (O3, O6) on the "Top"

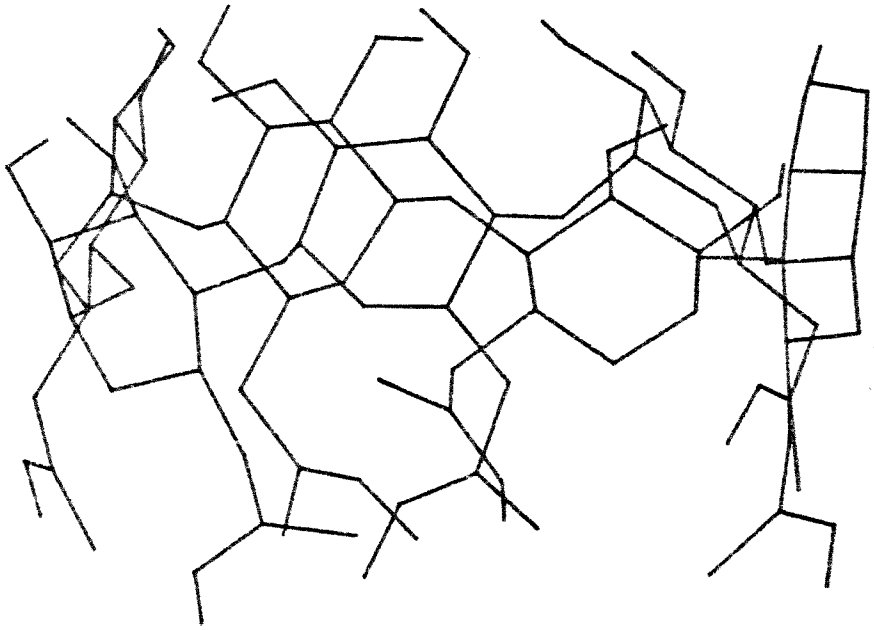

Caps are not all pointing into cavity

Figure 20.

Side view of minimized capped B-CD macrocycle, showing secondary hydroxyl oxygens. The secondary hydroxyl oxygens are in the O3 and O6 positions shown in Figure 13.

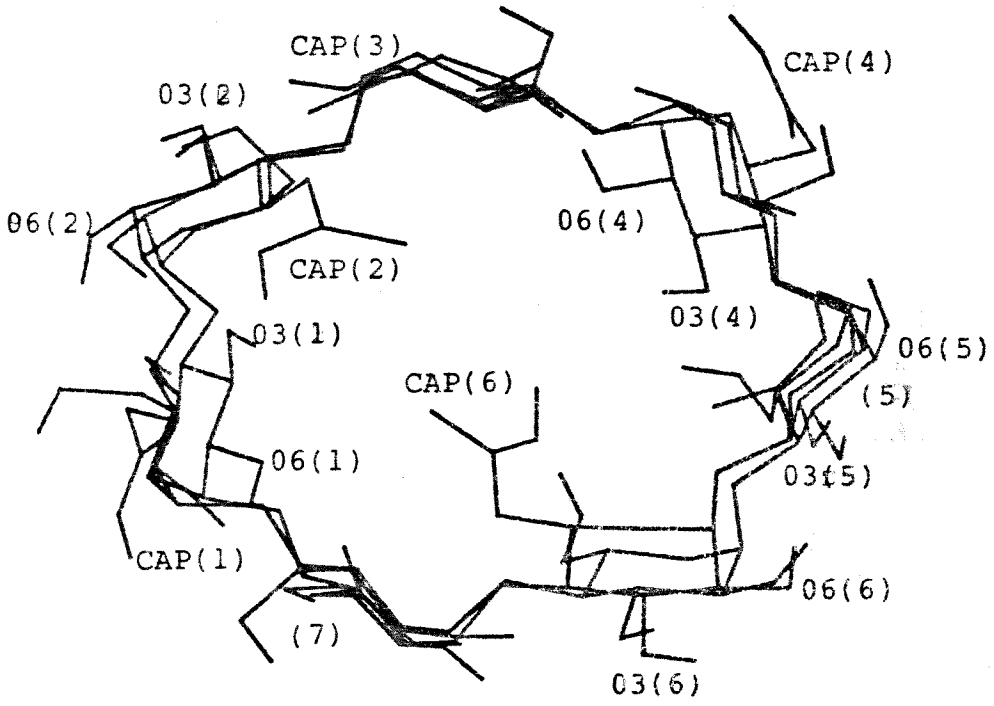

Figure 21.

Fit of X-ray B-CD macrocycle to the minimized capped B-CD macrocycle. Scaling parameters used were NB = 1.0, and EEL = 1.0. The secondary oxygens (O3, O6) of capped B-CD are in a different orientation when compared to the secondary oxygens (O3, O6) of the X-ray macrocycle. Fragment numbers are given in parentheses. Both the B-CD X-ray structure and the capped B-CD structure are shown in Figure 21.

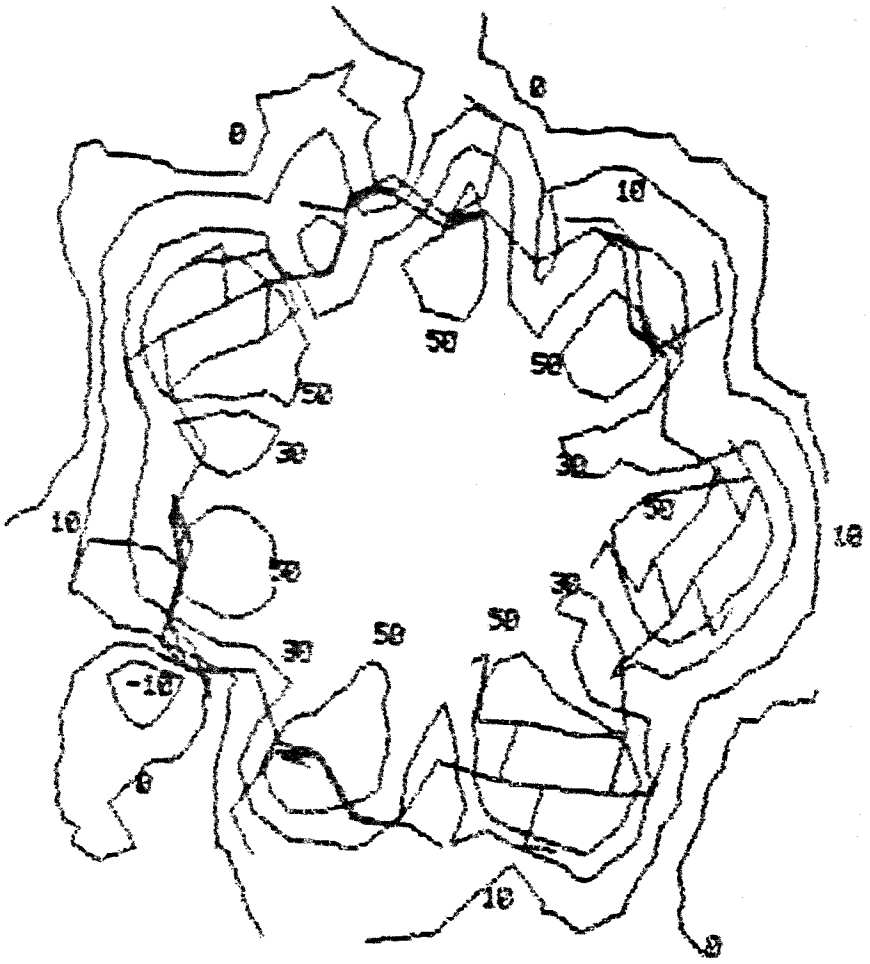

Figure 22.

Electrostatic potential for minimized B-CD macrocycle at z = 0 A. The values of the equi-energy contours are indicated on the map. The units are kcal/mole. The molecule is oriented with the glycosidic oxygens in the x-y plane at approximately z = 0 A. The secondary oxygens (O3,O6) are along the negative z-direction, while the primary oxygen, (O11) is along the positive z-direction.

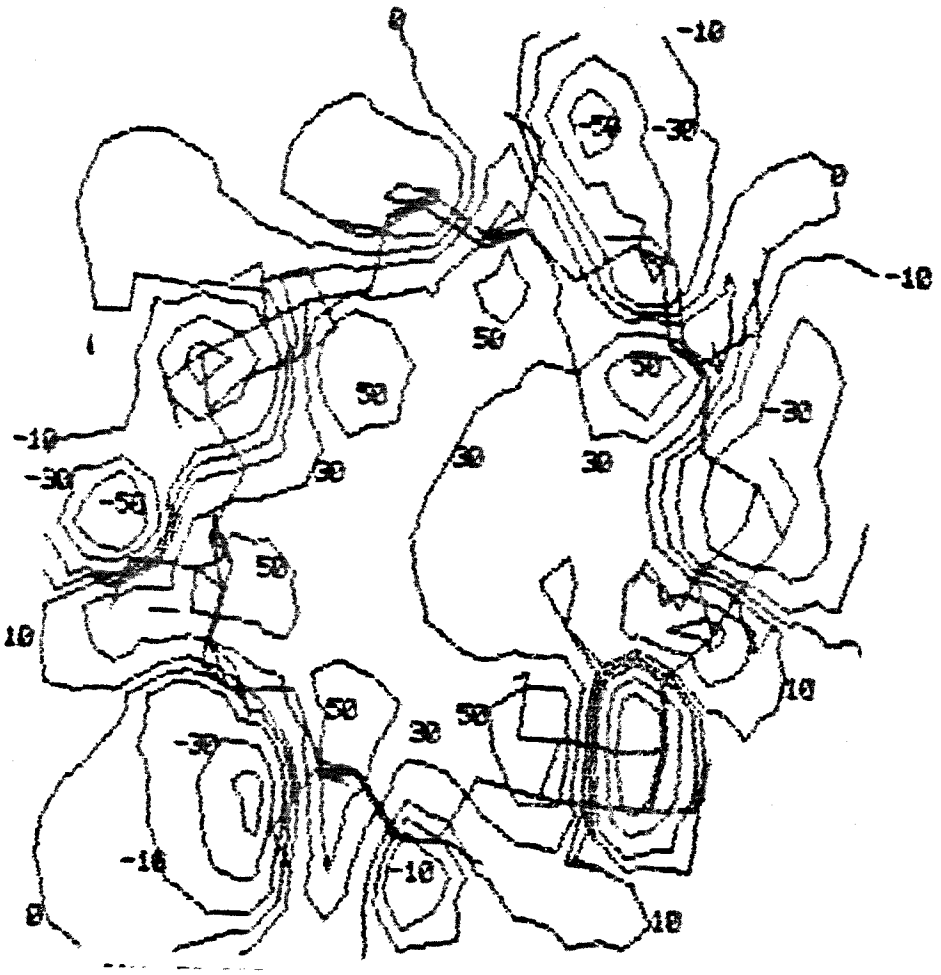

Figure 23.

Electrostatic potential for minimized B-CD macrocycle at z = 2 A. The values of the equi-energy contours are indicated on the map. The units are kcal/mole. The molecule is oriented with the glycosidic oxygens in the x-y plane at approximately z = 0 A. The secondary oxygens (O3,O6) are along the negative z-direction, while the primary oxygen, (O11) is along the positive z-direction.

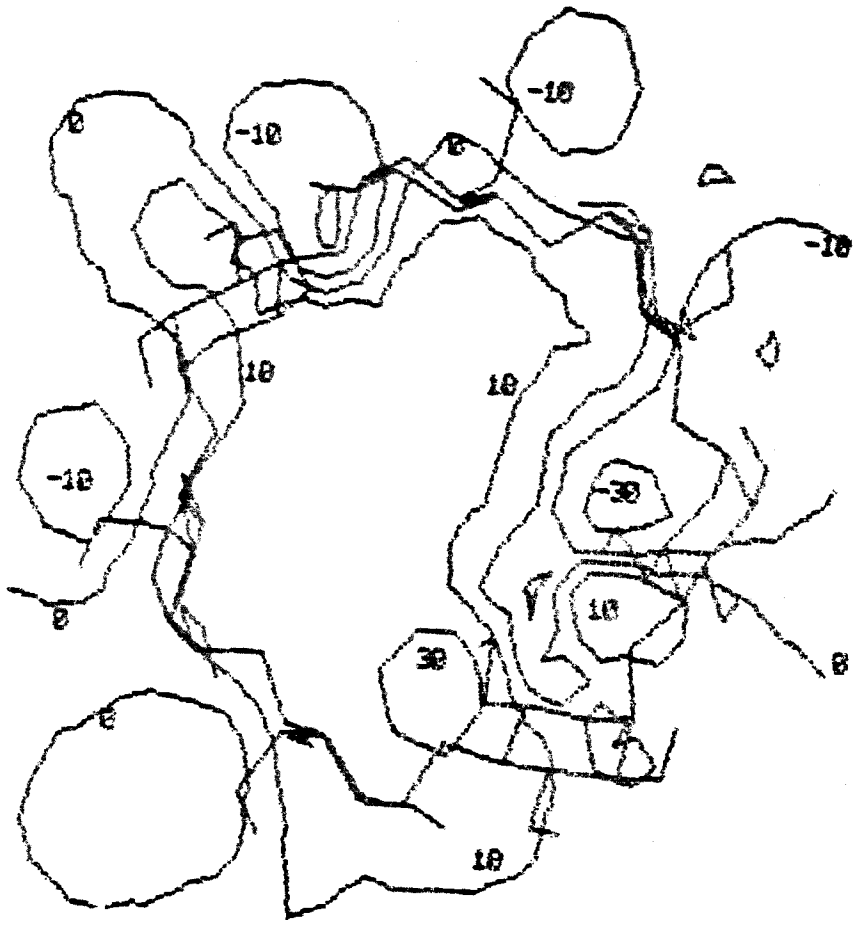

Figure 24.

Electrostatic potential for minimized B-CD macrocycle at z = 4 A. The values of the equi-energy contours are indicated on the map. The units are kcal/mole. The molecule is oriented with the glycosidic oxygens in the x-y plane at approximately z = 0 A. The secondary oxygens (O3,O6) are along the negative z-direction, while the primary oxygen, (O11) is along the positive z-direction.

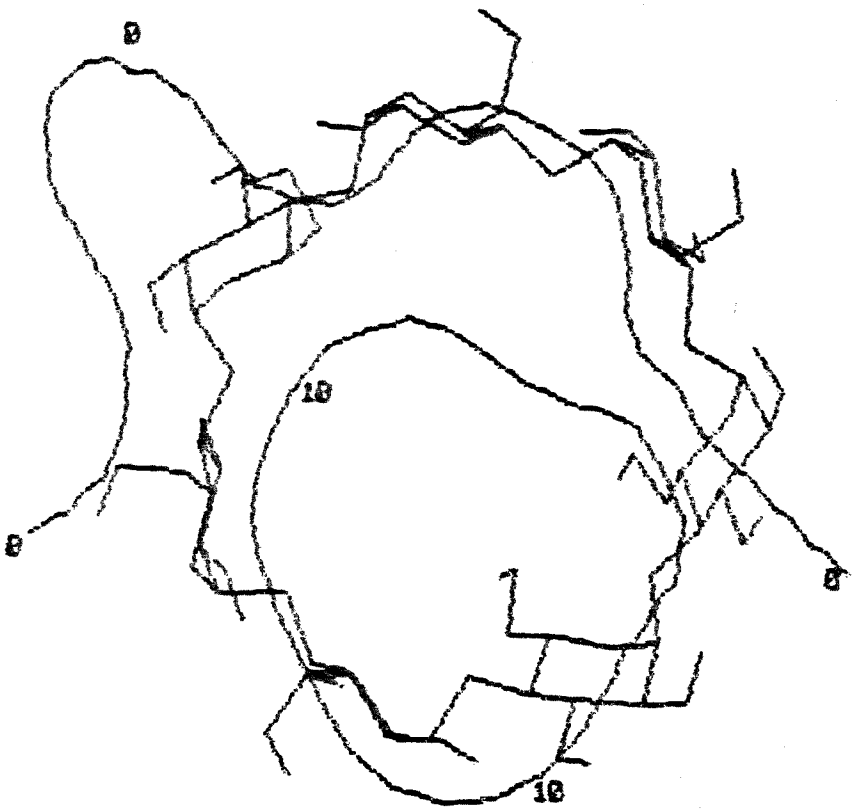

Figure 25.

Electrostatic potential for minimized B-CD macrocycle at z = 6 A. The values of the equi-energy contours are indicated on the map. The units are kcal/mole. The molecule is oriented with the glycosidic oxygens in the x-y plane at approximately z = 0 A. The secondary oxygens (O3,O6) are along the negative z-direction, while the primary oxygen, (O11) is along the positive z-direction.

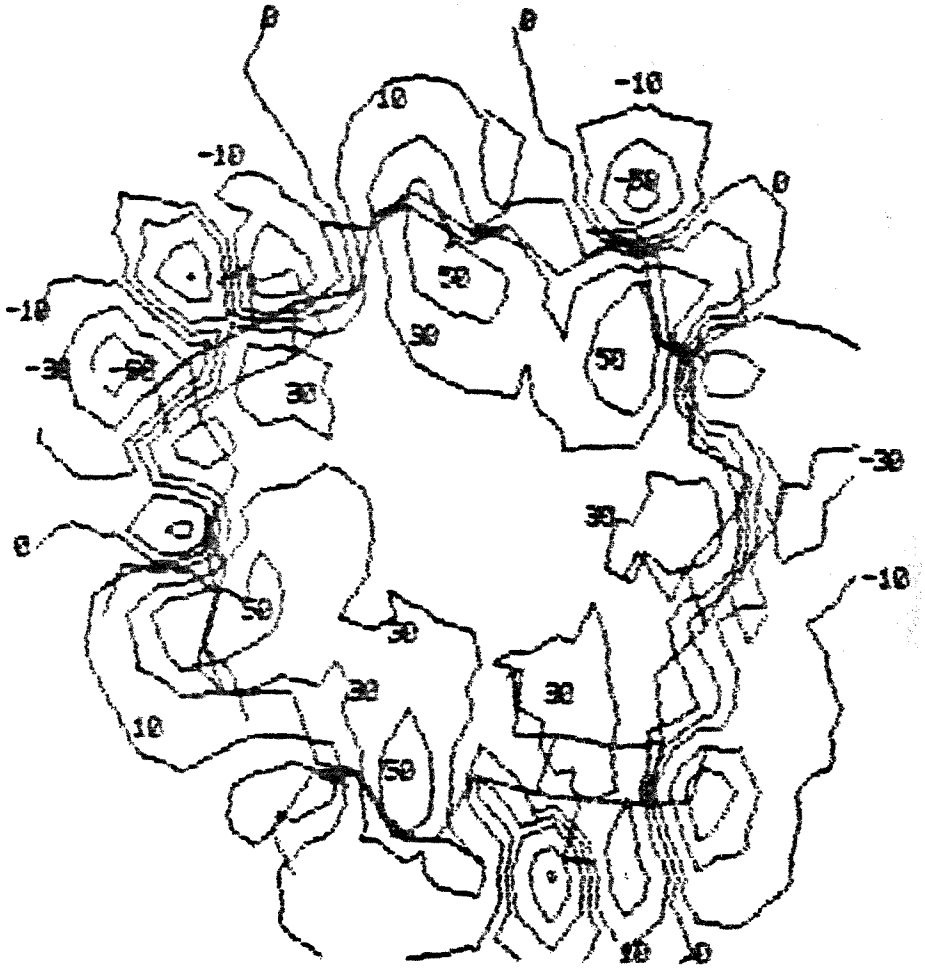

Figure 26.

Electrostatic potential for minimized B-CD macrocycle at z = -2 A. The values of the equi-energy contours are indicated on the map. The units are kcal/mole. The molecule is oriented with the glycosidic oxygens in the x-y plane at approximately z = 0 A. The secondary oxygens (O3,O6) are along the negative z-direction, while the primary oxygen, (O11) is along the positive z-direction.

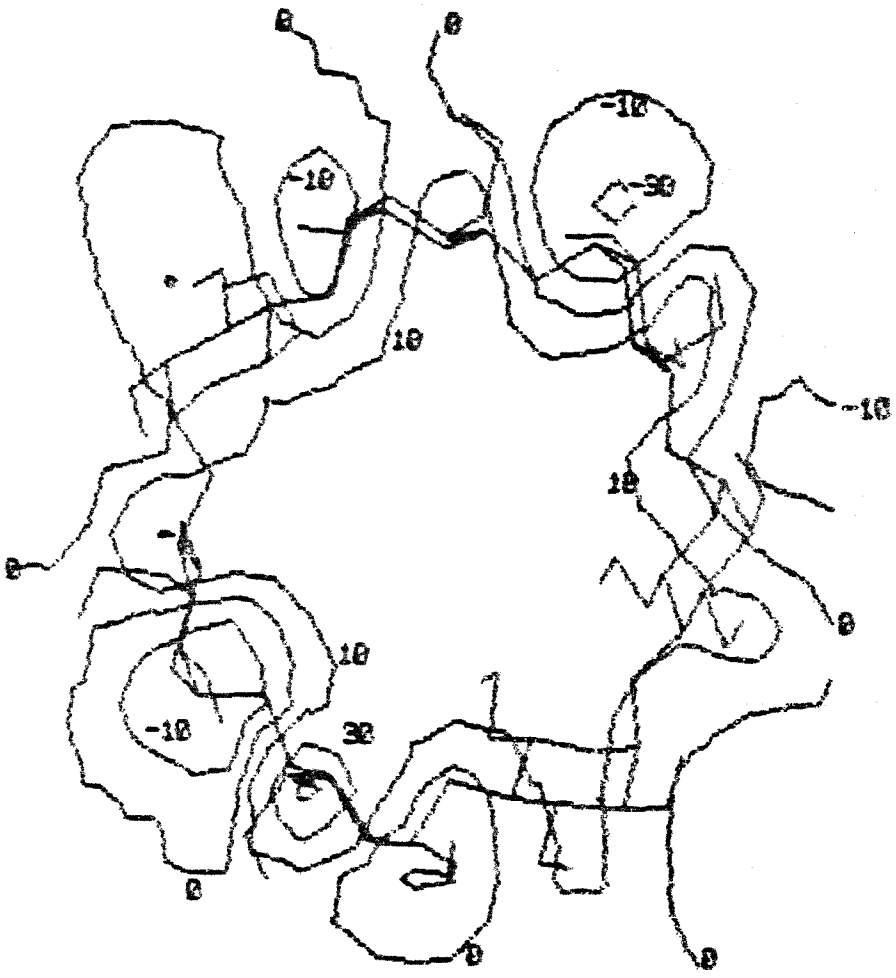

Figure 27.

Electrostatic potential for minimized B-CD macrocycle at z = -4 A. The values of the equi-energy contours are indicated on the map. The units are kcal/mole. The molecule is oriented with the glycosidic oxygens in the x-y plane at approximately z = 0 A. The secondary oxygens (O3,O6) are along the negative z-direction, while the primary oxygen, (O11) is along the positive z-direction.

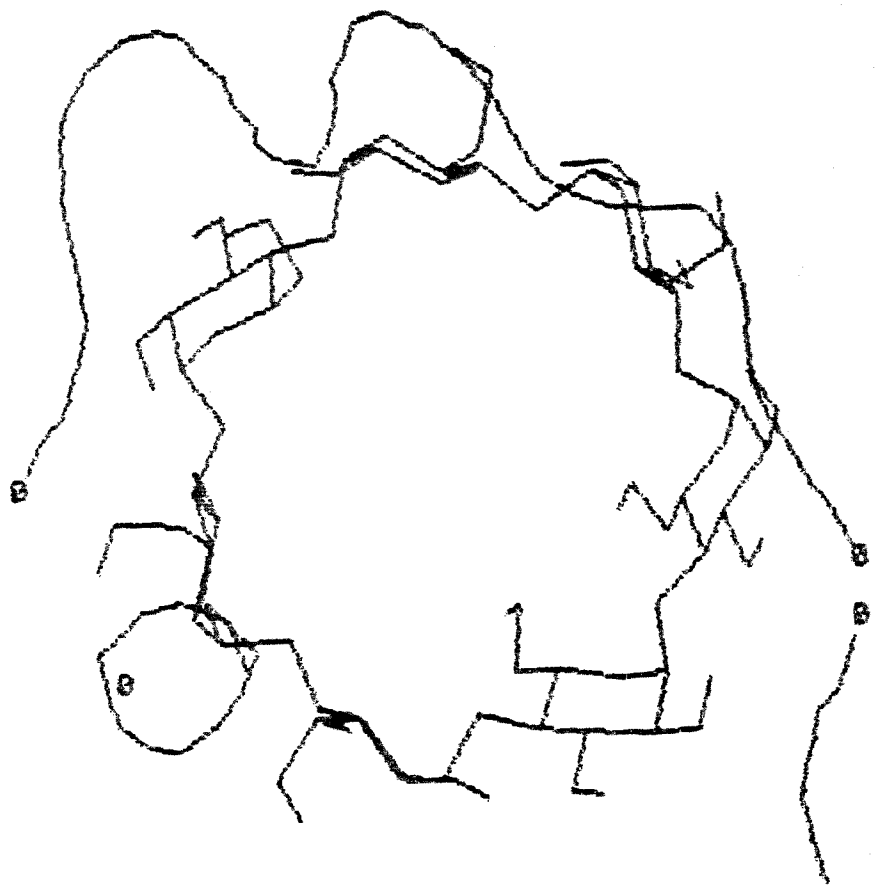

Figure 28.

Electrostatic potential for minimized B-CD macrocycle at z = -6 A. The values of the equi-energy contours are indicated on the map. The units are kcal/mole. The molecule is oriented with the glycosidic oxygens in the x-y plane at approximately z = 0 A. The secondary oxygens (03,06) are along the negative z-direction, while the primary oxygen, (011) is along the positive z-direction.

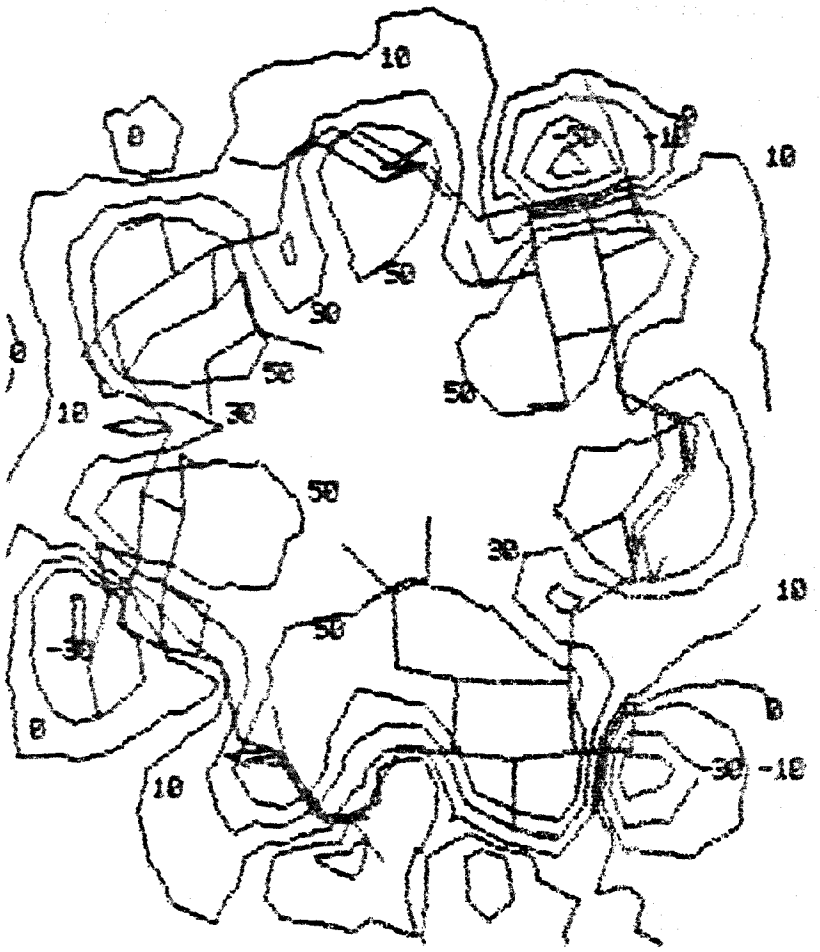

Figure 29.

Electrostatic potential contour map for minimized capped B-CD macrocycle at z = 0 A. The values of the equi-energy contours are indicated on the map. The units are kcal/mole. The molecule is oriented with the glycosidic oxygens in the x-y plane at approximately z = 0 A. The secondary oxygens (O3,O6) are along the negative z-direction, while the caps are along the positive z-direction.

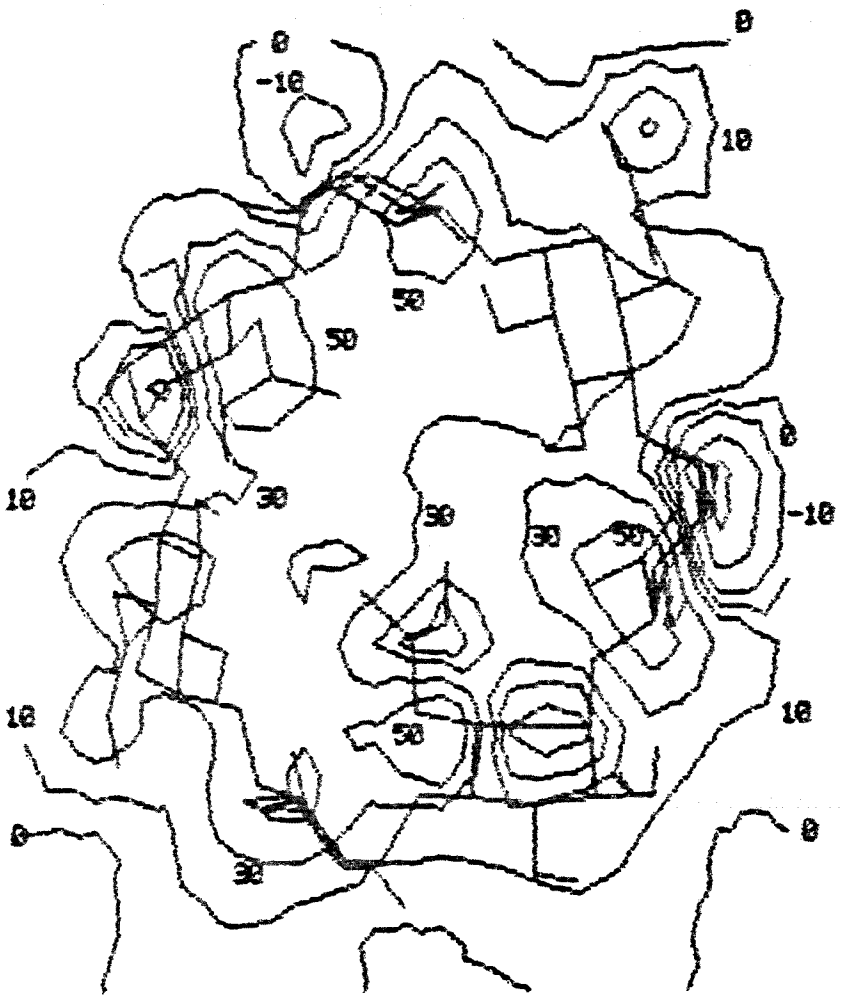

Figure 30.

Electrostatic potential contour map for minimized capped B-CD macrocycle at z = 2 A. The values of the equi-energy contours are indicated on the map. The units are kcal/mole. The molecule is oriented with the glycosidic oxygens in the x-y plane at approximately z = 0 A. The secondary oxygens (O3,O6) are along the negative z-direction, while the caps are along the positive z-direction.

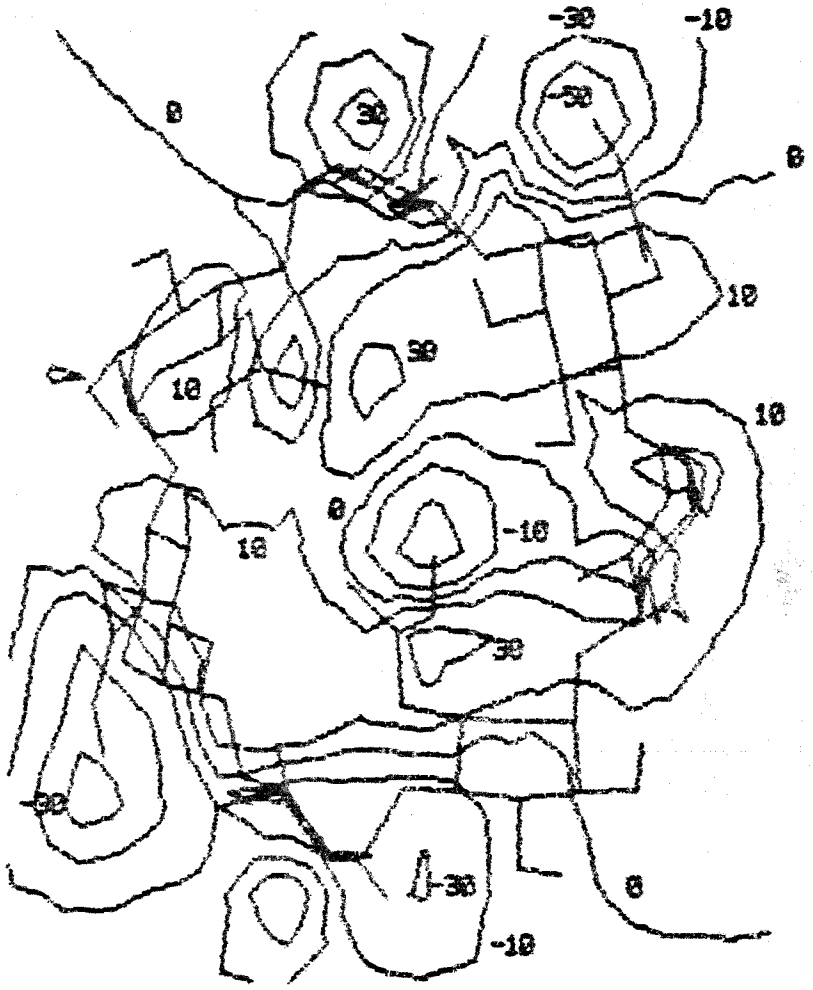

Figure 31.

Electrostatic potential contour map for minimized capped B-CD macrocycle at z = 4 A. The values of the equi-energy contours are indicated on the map. The units are kcal/mole. The molecule is oriented with the glycosidic oxygens in the x-y plane at approximately z = 0 A. The secondary oxygens (O3,O6) are along the negative z-direction, while the caps are along the positive z-direction.

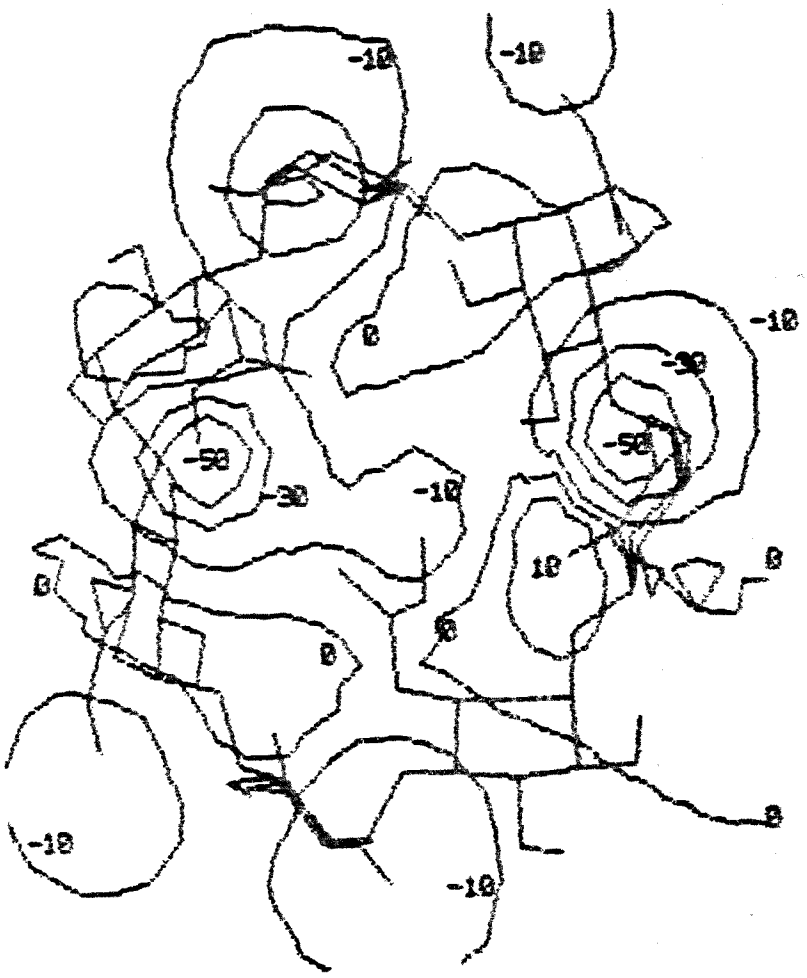

Figure 32.

Electrostatic potential contour map for minimized capped B-CD macrocycle at z = 6 A. The values of the equi-energy contours are indicated on the map. The units are kcal/mole. The molecule is oriented with the glycosidic oxygens in the x-y plane at approximately z = 0 A. The secondary oxygens (O3,O6) are along the negative z-direction, while the caps are along the positive z-direction.

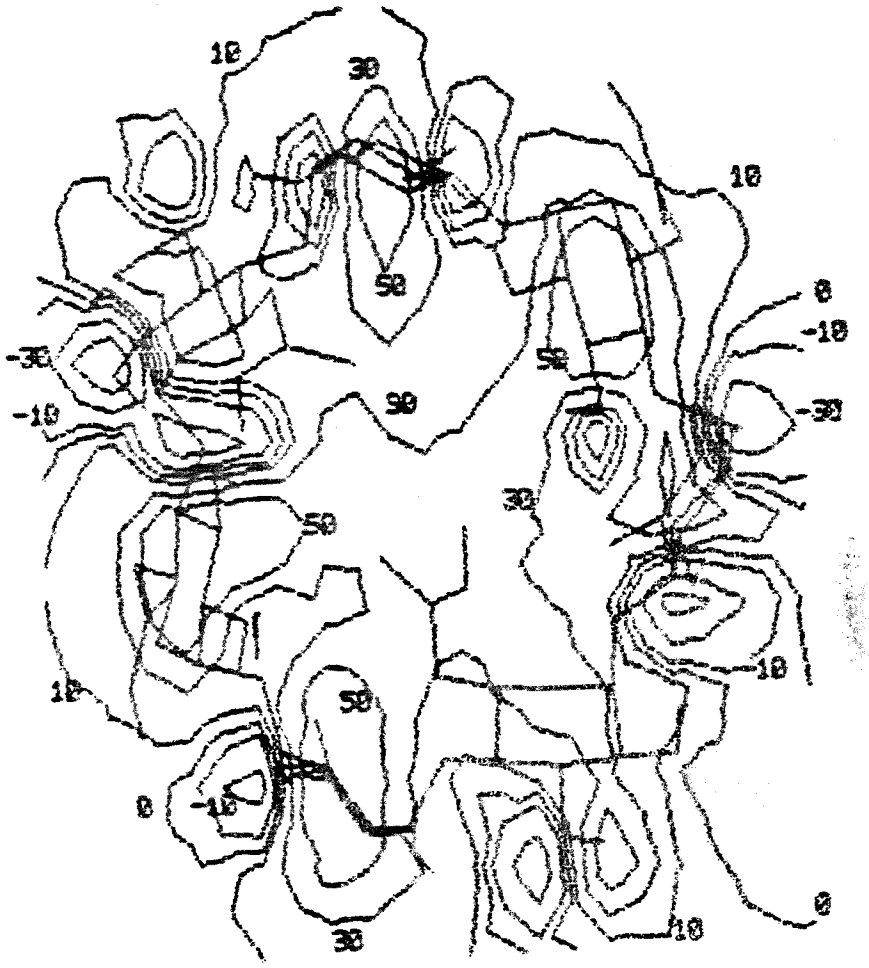

Figure 33.

Electrostatic potential contour map for minimized capped B-CD macrocycle at z = -2 A. The values of the equi-energy contours are indicated on the map. The units are kcal/mole. The molecule is oriented with the glycosidic oxygens in the x-y plane at approximately z = 0 A. The secondary oxygens (O3,O6) are along the negative z-direction, while the caps are along the positive z-direction.

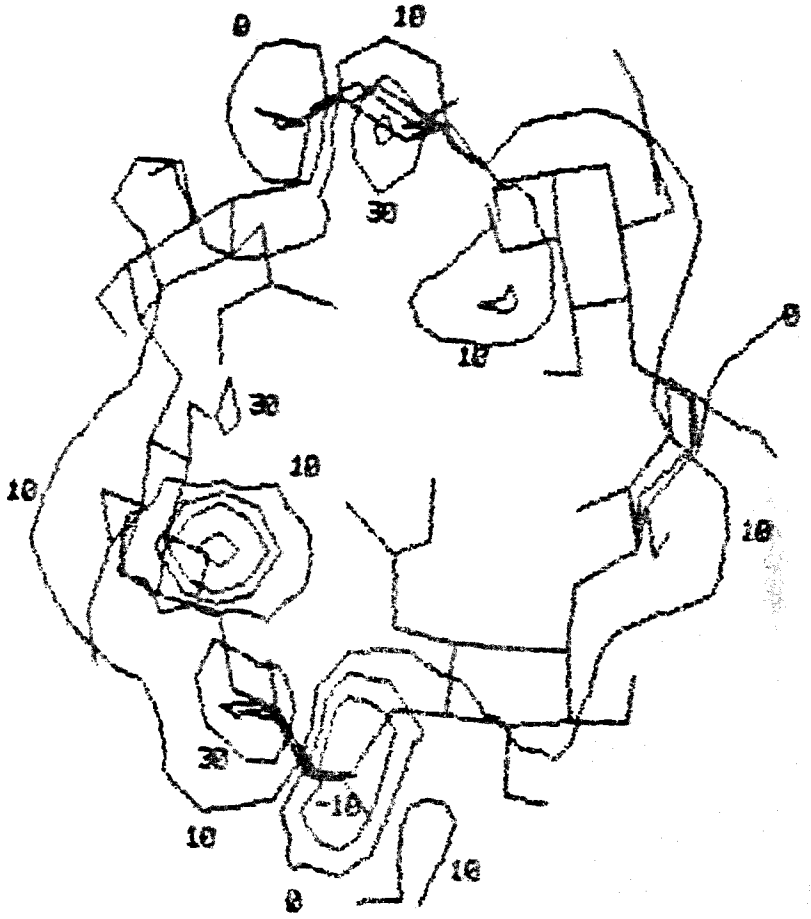

Figure 34.

Electrostatic potential contour map for minimized capped B-CD macrocycle at z = -4 A. The values of the equi-energy contours are indicated on the map. The units are kcal/mole. The molecule is oriented with the glycosidic oxygens in the x-y plane at approximately z = 0 A. The secondary oxygens (O3,O6) are along the negative z-direction, while the caps are along the positive z-direction.

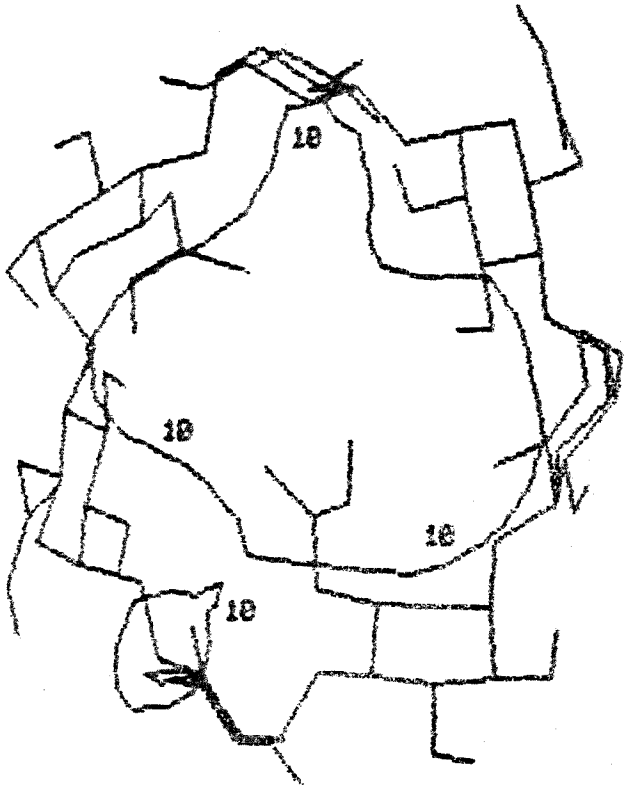

Figure 35.

Electrostatic potential contour map for minimized capped B-CD macrocycle at z = -6 A. The values of the equi-energy contours are indicated on the map. The units are kcal/mole. The molecule is oriented with the glycosidic oxygens in the x-y plane at approximately z = 0 A. The secondary oxygens (O3,O6) are along the negative z-direction, while the caps are along the positive z-direction.

BIBSER

The program BIBSER is used to search the bibliographic data file SBIB.DAT (system file) in order to provide references to structures of interest to the user.

Input File(s)

QBIB.DAT(user input)- contains the entry questions for the BIBSER search procedure. Run a maximum of five (5) questions in QBIB.DAT during interactive sessions, since this tends to tie up a terminal until the job is completed. For batch jobs, the number of questions is user dependent. See sample input in QBIB.DAT to BIBSER below.

QBIB.DAT

SAMPLE INPUT QUESTIONS

```
Q*DATE '750417'
Q *DATE '750101-760101'
Q *COMPND 'ADEN'
Q *COMPND 'HOMOMUSCIMOL'
Q *COMPND 'CONFIGURATION'
Q *FORMUL 'CA1'
Q *FORMUL 'C3'
Q *FORMUL 'B1 F4 -'
Q *FORMUL 'C35-40'
```

```
Q *FORMUL 'CR1-3'
Q *FORMUL '+++'
Q *ELEMENT 'B'
Q *ELEMENT 'PT&P&F'
Q *AUTHOR 'STRUCHKOV'
Q *CODEN '036'
Q *CODEN '036' AND *VOL '63'
Q *CODEN '036' AND *VOL '63' AND *PAGE '399'
Q *JRNL 'J.ORGANOMETAL.CHEM.'
Q *YEAR '73'
Q *YEAR '68-73'
Q *REFER '6.60.2
Q *REFER '6.60.10'
Q *CLASS '05'
Q *CLASS '01-05'
Q *CLASS '71-86' AND *ELEMENT 'PT'
Q *CLASS '86' NOT *ELEMENT 'AU' OR 'PD' OR 'PT'
Q *ELEMENT 'CU' OR 'AG' OR 'AU'  AND  *YEAR '74' NOT *CLASS
'83-86'
Q *ELEMENT 'TR'  NOT *CLASS '71-86'
Q *ELEMENT 'TR&S'
Q *ELEMENT 'LN'
```

Output Files

BIBSER.LC0-
contains the references (author's name,

journals, etc.) for each question submitted in QBIB.DAT. This file should be printed and/or deleted and then reviewed by the user to verify which refcode(s) is actually needed. See sample ouput from BIBSER below.

Start of sample output from BIBSER.

```
     INPUT...        Q *COMPND 'BETA' AND 'CYCLODEX'


 NUMBER OF QUESTIONS  1
 NUMBER OF STRINGS  2
 TOTAL NUMBER OF CHARACTERS  14


 * END OF FILE REACHED ON UNIT 1 *

 NUMBER OF ENTRIES SEARCHED = 50499

 NUMBERS OF HITS FOR QUESTIONS
    32
1
Q*COMPND'BETA' AND'CYCLODEX'
 ------------------------------------------------------
 QUESTION NUMBER  1  NHITS =  32

       "HIT NUMBER 1 FOR INPUT QUESTION"

 BETA-CYCLODEXTRIN DODECAHYDRATE

 C42 H70 O35, 12(H2 O1)

 BCDEXD    K.LINDNER,W.SAENGER,  ANGEW.CHEM.,INT.ED.ENGL.,
17,694,1978. 179 790214  10.45.65, 1/45
```

```
       "HIT NUMBER 2  FOR INPUT QUESTION"

 BETA-CYCLODEXTRIN DODECAHYDRATE (AT 120 DEG.K)

 CYCLOHEPTA-AMYLOSE DODECAHYDRATE

 C42 H70 O35, 12(H2 O1)
```

BCDEXD01 J.J.STEZOWSKI,J.M.MACLENNAN, AM.CRYST.ASSOC.,
SER.2, 7,24,1980. 395
800822 12.45.67, 1/45

"HIT NUMBER 3 FOR INPUT QUESTION"

BETA-CYCLODEXTRIN DODECAHYDRATE (REDETERMINATION USING
DIFFERENT CRYSTAL SAMPLE)
C42 H70 O35, 12(H2 O1)
BCDEXD02 T.FUJIWARA,M.YAMAZAKI,Y.TOMIZU,R.TOKUOKA,
K.-I.TOMITA,T.MATSUO,H.SUGA,W.SAENGER, NIPPON KAGAKU
KAISHI, ,181,1983. 361
840221 , 1/61,1/45

BIBSER.OUT- is a sub-directory of the matches found in SBIB.DAT. It is created only when the keyword FILE is used in QBIB.DAT, otherwise it is empty. Delete at earliest convenience.

REFCODE.DAT- is probably the most important file from BIBSER, since it is needed for the next program called RETRIEVE. REFCODE.DAT contains 6 digit refcodes(matches) that corresponds to each question in QBIB.DAT. As mentioned previously, edit REFCODE.DAT and delete the unneeded codes. See sample output from REFCODE.DAT below.

REFCODE.DAT

CAMPIP 1

```
BOYFOK11 1
BUVSEQ   1
```

CONNSER

This program is used to obtain connectivity data from SCONN.DAT (system file)

Input File(s)

QCONN.DAT(user input)- contains the connectivity data questions for the CONNSER search procedure. Run a maximum of five (5) for interactive sessions, and a maximum of 15 for batch sessions (possible to run more on batch, but it takes a prohibitive amount of time to complete). See sample input file to CONNSER below.

QCONN.DAT

```
Q CAPPED CYCLODEXTRIN W/METHYL FORMAMIDE
AT1 O 2
AT2 C 3 1
AT3 C 3 1
AT4 C 3 1
AT5 C 3 1
AT6 C 3 1
AT7 O 1
AT8 O 1 1
AT9 O 1 1
BO 1 2 1 C
BO 2 3 1 C
BO 3 4 1 C
BO 3 7 1 A
BO 4 5 1 C
BO 4 8 1 A
BO 5 6 1 C
BO 5 9 1 A
BO 6 1 1  C
END
```

Output File(s)

CONNSER.LC0-
contains the "hits" for the questions in QCONN. DAT. Analagous to BIBSER.LC0, therefore follow the same procedure.

CONNSER.OUT-
is very similar to BIBSER.OUT, therefore follow similar procedure.

REFCODE.DAT-
same file as that produced in the BIBSER run, ergo same procedure.

RETRIEVE

This program is used to obtain file entries from system files RDAT.DAT and DATA.DAT.

Input File(s)

RETRIEVE.DAT(user input)-
instructs the program RETRIEVE as to which file to open, depending on the keyword used. See sample input file to RETRIEVE below.

RETRIEVE.DAT

RDAT

REFCODE.DAT-

is the output file from BIBSER or CONNSER.

Output File(s)

RETRIEVE.LC0-
contains a sub-listing of the SBIB, SCONN, or RDAT entries. Delete at first opportunity.

RETRIEVE.OUT-
contains the geometry information(bond lengths and angles etc.). It is used in the next program called GEOM78.

GEOM78

This program is used to output the geometric properties in formatted output. In addition, it can also give cartesian coordinates if the correct keyword is used.

Input Files

GEOM78.DAT(user input)-
contains the keyword instructions for GEOM78. The default for GEOM78.DAT, a blank file, is to calculate geometric properties. See sample input file to GEOM78 below.

GEOM78.DAT

OUTPUT COORDS

RETRIEVE.OUT-
is the output file from RETRIEVE.

Output Files

GEOM78.LC0-
contains the geometric properties (bond angles etc.) for each refcode.

GEOM78.OUT-
contains cartesian coordinates which are preceded by its respective refcode, for all hits.

SUMMARY

BIBSER-> TO RUN BIBSER, YOU SIMPLY NEED QBIB.DAT IN YOUR MAIN DIRECTORY. ONCE THAT IS DONE, R PUB$CAMB:BIBSER

CONNSER-> TO RUN CONNSER, YOU SIMPLY NEED QCONN.DAT IN YOUR MAIN DIRECTORY. THEN SIMPLY: R PUB$CAMB:CONNSER

RETRIEVE-> MAKE SURE REFCODE.DAT AND RETRIEVE.DAT ARE IN YOUR DIRECTORY. THEN: R PUB$CAMB:RETRIEVE

GEOM78-> VERIFY THAT RETRIEVE.OUT AND GEOM78.DAT ARE IN DIRECTORY. THEN R PUB$CAMB:GEOM78

NOTE: If any problems occurs with the executing command, then use the more formal command, which is: RUN [PUBLIC.ACS.CAMBRIDGE]FILENAME.

VIII. BIBLIOGRAPHY

[1] Dugas, H.; Penney, C. Bioorganic Chemistry; A Chemical Approach to Enzyme Action; Springer-Verlag: New York, 1981; Chapter 4.

[2] Breslow, R. Science 1982, 218, 5.

[3] (a) Komiyama, M.; Bender, M.L. Bull. Chem. Soc. Jpn. 1980, 53, 1073. (b) Komiyama, M.; Bender, M.L. The Chemistry of Enzyme Action; Page M.I. Ed.; Elsevier: New York, 1984; Vol.6, Chapter 14, pp. 505-527.

[4] Breslow, R.; Czarniecki M.F.; Emert, J.; Hamaguchi, H. J. Am. Chem. Soc. 1980, 102, 762-769.

[5] (a) Cram, D.J.; Dicker, I.B.; Knobler, C.B.; Trueblood, K.N. J. Am. Chem. Soc. 1984, 106, 7150; (b) Cram, D.J.; Katz, H.E. J. Am. Chem. Soc., 1983, 105, 135-137; (c) Cram, D.J.; Lam, P. Y.-S.; Ho, S.P. J. Am. Chem. Soc., 1986, 108, 839-841.

[6] Stryer, L. Biochemistry; W.H. Freeman and Co.: San Francisco, 1981; pp. 158-165.

[7] Walsh, C. Enzymatic Reaction Mechanisms; W.H. Freeman and Co.: San Francisco, 1979, pp. 56-97.

[8] (a) Venanzi, C.A.; Bunce, J.D. Int. J. Quantum Chem. 1986, QBS12, 69-87; (b) Venanzi, C.A.; Bunce, J.D. Ann. N.Y. Acad. Sci., 1986, 471, 318-320.

[9] Venanzi, C.A.; Bunce, J.D. Enzyme 1986, 36, 79-92.

[10] Venanzi, C.A. Molecular Structure and Energetics, 9, (Principles of Enzyme Activity), Liebman, J.F; Greenberg, A. Eds.; VCH Publishers: Deerfield Beach, Florida, in press.

[11] Chemical Applications of Atomic and Molecular Electrostatic Potentials. Politzer, P.; Truhlar, D.G. Eds.; Plenum Press: New York, 1981.

[12] Bender, M.L.; Bergeron, R.J.; Komiyama, M. The Bioorganic Chemistry of Enzyme Catalysis; John Wiley and Sons: New York, 1984, Chapter 12.

[13] Saenger, W. Angew. Chem. Int. Ed. (Engl.) 1980, 19, 344-362.

[14] Komiyama, M.; Inoue, S. Bull. Chem. Soc. Jpn. 1980, 53, 3334.

[15] Komiyama, M.; Bender, M.L. J. Am. Chem. Soc. 1977, 99, 8021-8024 .

[16] Bender, M.L.; Komiyama, M. Cyclodextrin Chemistry; Springer-Verlag: Berlin, 1978.

[17] Weiner, P.K.; Kollman, P.A. J. Comp. Chem. 1981, 2, 287 - 303.

[18] Davies, E.K. : Chem-X; Chemical Crystallographic Laboratory, Oxford University (Chemical Design Ltd., Oxford, UK).

[19] Harata, K. Bull. Chem. Soc. Jpn. 1982, 55, 2315 - 2320.

[20] Allen, F.H.; Kennard, O. Perspectives in Computing 1983, 3, 28 - 43.

[21] Dewar, M.S.; Thiel, W. J. Am. Chem. Soc. 1977, 99, 4899-4907.

[22] Stewart, J.J.P.: MOPAC: A general molecular orbital package. Quantum Chemistry Program Exchange Bull. 1983, 3, 43.

[23] Singh, U.C.; Kollman, P. "GAUSSIAN 80 UCSF", Quantum Chemistry Program Exchange Bull. 1982, 2, 17.

[24] Weiner, S.J.; Kollman, P.A.; Case,D.A.; Singh, U.C.; Alagona, G.; Profeta Jr., S.; Weiner, P. J. Amer. Chem. Soc. 1984, 106, 765-784.

[25] (a) Wipff, G.; Weiner, P.; Kollman, P. J. Amer. Chem. Soc. 1982, 104, 3249-3258; (b) Kollman, P.A.; Wipff, G.; Singh, U.C. J. Am. Chem. Soc., 1985, 107, 2212-2219.

[26] Singh, U.C.; Kollman, P.A. J. Comp. Chem. 1984, 5, 129-145.

[27] Weiner, P. Modification of RMS Module of AMBER, 1986.

[28] Fersht, A. Enzyme Structure and Mechanism; W.H. Freeman and Co.: Reading, 1977; p. 230.

[29] Klar, B.; Hingerty, B.; Saenger, W. Acta. Cryst., 1980, B36, 1154-1165.

[30] Koehler, J.; Saenger, W.; van Gunsteren, W.F. "A Molecular Dynamics Simulation of Crystalline alpha-Cyclodextrin Hexahydrate", in press.

[31] Morrison, R.T.; Boyd, R.N. Organic Chemistry; Allyn and Bacon,Inc.: Boston, 1983; p. 474.